6. Subsonic Aerodynamics of Airfoils and Wings

6.1 Introduction

In this chapter we discuss the subsonic aerodynamics of airfoils and wings. We look at the basic aerodynamics mainly from an inviscid point of view. Generally, this is a reasonable starting point for thinking about aerodynamics in attached flow. Traditionally, the methods used to make these calculations are generally known as panel methods and vortex lattice methods. The theory is described in the notes for Applied Computational Aerodynamics, Chapters 4 and 6. Although we are addressing the aerodynamic features, we will provide brief overviews of the methods used to compute the results shown.

One of the key features of subsonic flow is the use of Laplace's Equation as the basis for the inviscid solution. Solutions are found using this linear equation through superposition of "singularities" of unknown strength which are distributed over discretized portions of the surface: *panels*. Hence the flowfield solution is found by representing the surface by a number of panels, and solving a linear set of algebraic equations to determine the unknown strengths of the singularities.* An entry into the panel method literature is available through two recent reviews by Hess,[1,2] the survey by Erickson,[3] and the book by Katz and Plotkin.[4]

A more approximate, yet physically appealing, approach is often used to compute wing aerodynamics. In this approach the wing is represented by a system of horseshoe vortices placed on the mean surface. These methods are known as vortex lattice methods (**VLM**). Generally they ignore the thickness effects. This is possible because for relatively thin surfaces the effects of thickness cancel between the upper and lower surfaces, so that the lift is not influenced by the thickness to first order. We will illustrate wing aerodynamics using vortex lattice methods. A key reference for these methods is a workshop devoted to these methods at NASA in the mid '70s.[5] A nearly universal standard for vortex lattice predictions had been established by then. It was a code developed at NASA Langley by Rich Margason, John Lamar and co-workers.[6,7,8,9]

Chapter 6 of *Applied Computational Aerodynamics* provides complete details on the **VLM** method, together with references to other implementations of the method. Some of the most noteworthy variations on the basic method have been developed by Lan[10] (Quasi-Vortex Lattice Method), Hough[11], DeJarnette[12] and Frink.[13] Mook[14] and co-workers at Virginia Tech have developed vortex lattice class methods that treat flowfields that contain leading edge vortex type separation and also handle general unsteady motions and deforming wakes. The recent book by

* The singularities are distributed across the panel. They are not specified at a point. However, the boundary conditions usually are satisfied at specific locations.

Katz and Plotkin[4] contains another variation. At Virginia Tech, Jacob Kay wrote a code using the method of Katz and Plotkin to estimate stability derivatives, which is available from our software web site.[15] Two other vortex lattice methods have emerged more recently. Tornado is a MatLab code developed in Sweden, [16]and AVL by Prof. Drela and Harold Youngren has been made publicly available recently. [17]

6.2 Airfoils

The results presented here mainly use program **PANEL**.[18] It is an inviscid flowfield solution. However, the current standard program for subsonic airfoil analysis and design is due to Prof. Mark Drela of MIT and is known as **XFOIL**.[19] It includes viscous effects and is in the public domain for academic use. See their software web site for access to this code and more details.

6.2.1 Program PANEL and other prediction methods: Accuracy and Validation

Most of the results presented in this section were computed using program **PANEL.** This is essentially the program given by Moran.[18] Program **PANEL's** node points are distributed employing the widely used cosine spacing function. This approach is used to provide a smoothly varying distribution of panel node points that concentrate points around the leading and trailing edges. An example of the accuracy of program **PANEL** is given in Figure 6-1, where the results from **PANEL** for the NACA 4412 airfoil are compared with results obtained from an exact conformal mapping of the airfoil (which can be considered to be an exact solution). The agreement is nearly perfect.

Before using any program, the code must be verified by the user. Numerical studies need to be conducted to determine, for a panel method program, how many panels are required to obtain accurate results. Both forces and moments and pressure distributions should be examined. Most codes require that you select the number of panels used to represent the surface. How many should you use? One of the first things the user should do is evaluate how detailed the calculation should be to obtain the level of accuracy desired.

We check the sensitivity of the solution to the number of panels by comparing force and moment results and pressure distributions with increasing numbers of panels. To estimate the limit for a large number of panels the results can be plotted as a function of the reciprocal of the number of panels. Thus the limit result occurs as $1/n$ goes to zero. Figures 6-2 through 6-4 present the results in this manner for the case given above, and with the pitching moment included for examination in the analysis. We see in Figure 6-2 that the drag is approaching zero, which is the correct result for a two-dimensional inviscid incompressible solution.

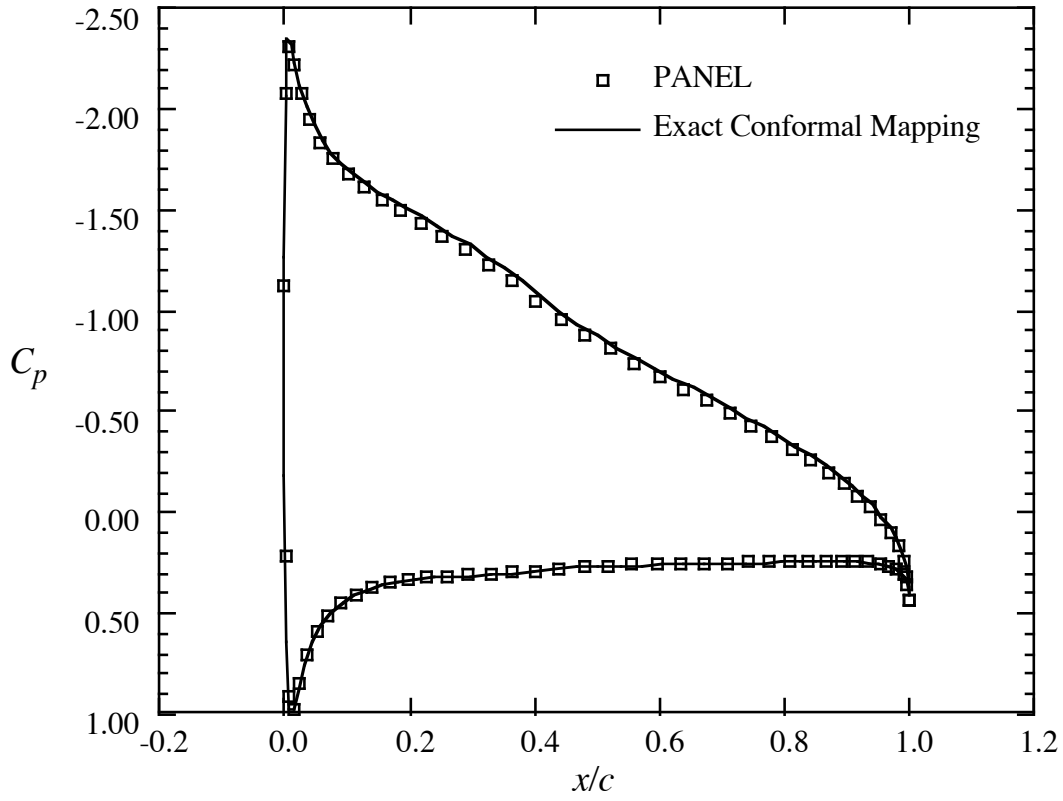

Figure 6-1. Comparison of results from program **PANEL** with an essentially exact mapping solution for the NACA 4412 airfoil at 6° angle-of-attack.

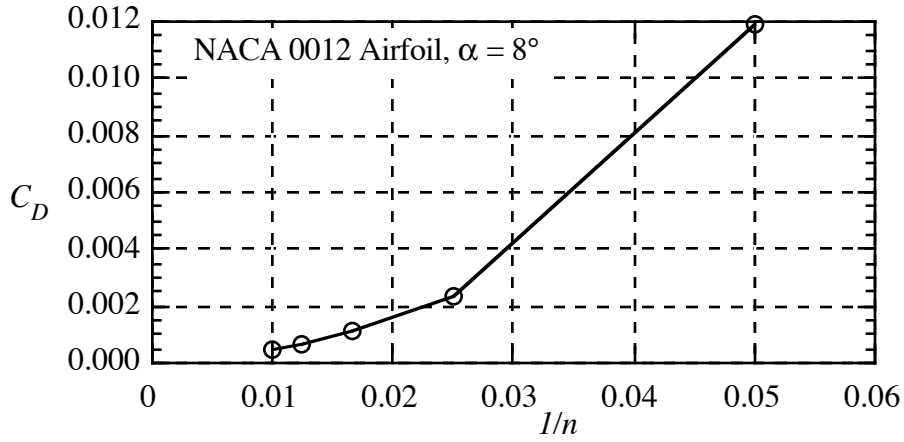

Figure 6-2. Change of drag with the inverse of the number of panels.

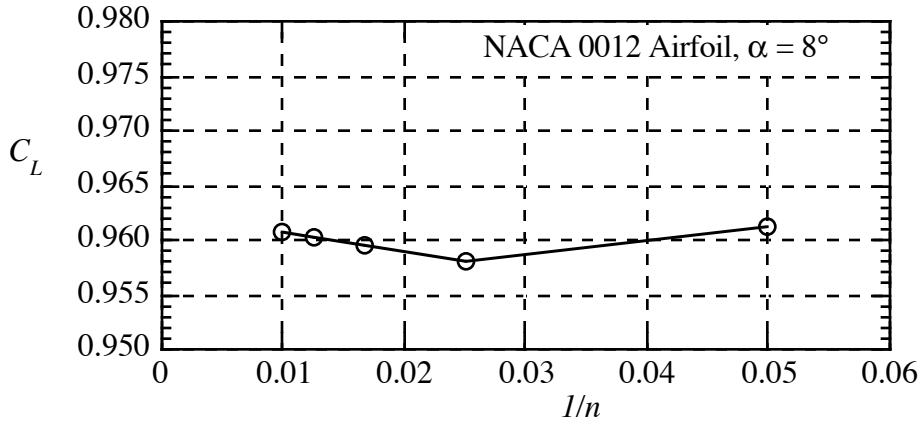

Figure 6-3. Change of lift with the inverse of the number of panels.

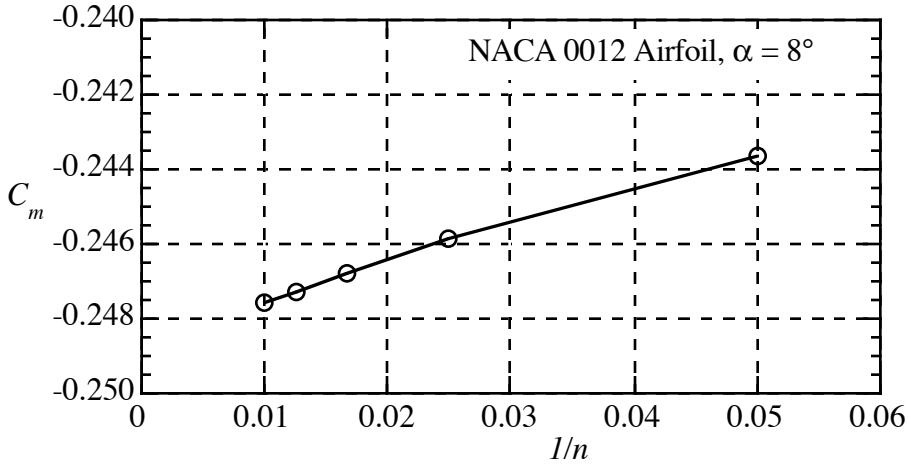

Figure 6-4. Change of pitching moment with the inverse of the number of panels.

The results given in Figures 6-2 through 6-4 show that program **PANEL** produces results that are relatively insensitive to the number of panels once fifty or sixty panels are used, and by extrapolating to $1/n = 0$ an estimate of the limiting value can be obtained.

In addition to forces and moments, the sensitivity of the pressure distributions to changes in panel density should also be investigated. Pressure distributions are shown in Figures 6-5 and 6-6. Figure 6-5 contains a comparison between the 20 and 60 panel cases. In this case it appears that the pressure distribution is well defined with 60 panels. This is confirmed in Figure 6-6, which demonstrates that it is almost impossible to identify the differences between the 60 and 100 panel cases. This type of study should (*in fact* ***must***) be conducted when using computational aerodynamics methods.

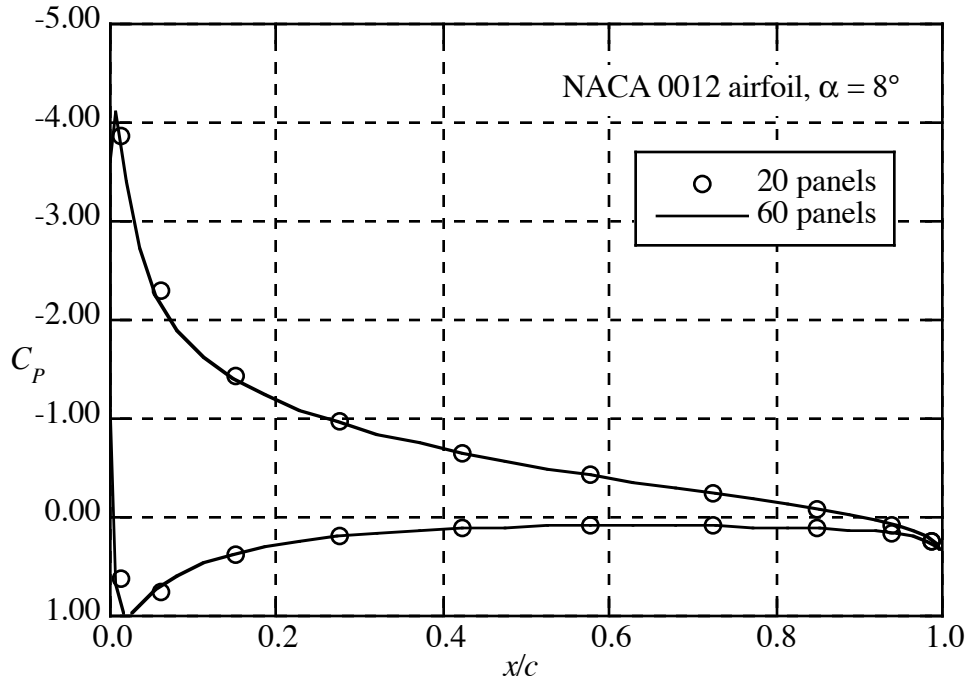

Figure 6-5. Pressure distribution from program **PANEL**, comparing results using 20 and 60 panels.

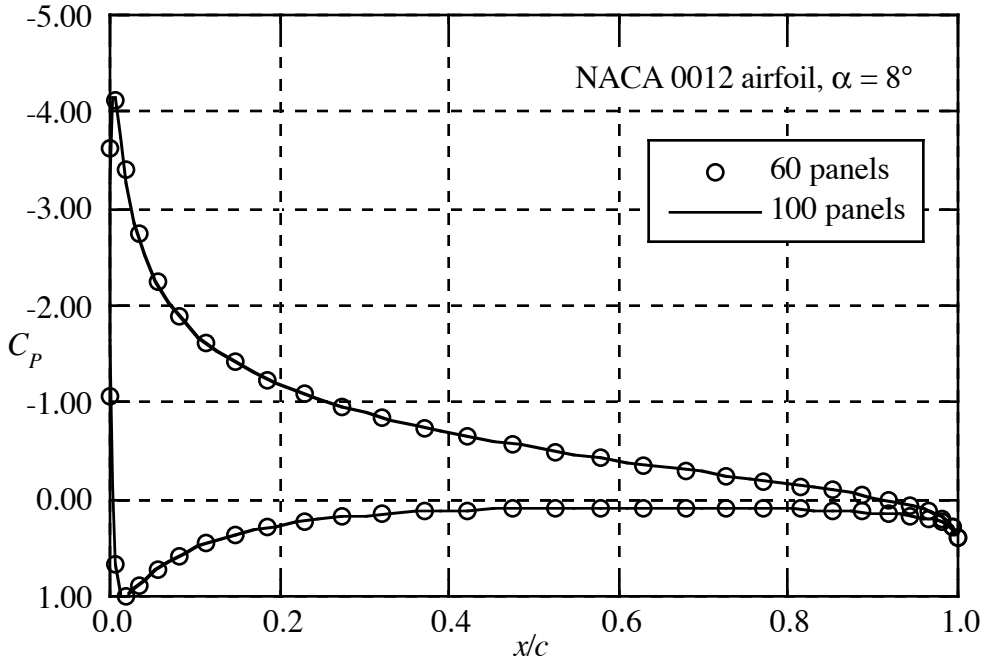

Figure 6-6. Pressure distribution from program **PANEL**, comparing results using 60 and 100 panels.

Having examined the convergence of the mathematical solution, we investigate the agreement with experimental data. Figure 6-7 compares the lift coefficients from the inviscid solutions obtained from **PANEL** with experimental data from Abbott and von Doenhoff.[20] Agreement is good at low angles of attack, where the flow is fully attached. The agreement deteriorates as the angle of attack increases, and viscous effects start to show up as a reduction in lift with increasing angle of attack, until, finally, the airfoil stalls. The inviscid solutions from **PANEL** cannot capture this part of the physics. There are significant differences in the airfoil behavior at stall between the cambered and uncambered airfoil. Essentially, the differences arise due to different flow separation locations on the different airfoils. The cambered airfoil separates at the trailing edge first. Stall occurs gradually as the separation point moves forward on the airfoil with increasing incidence. The uncambered airfoil stalls due to a sudden separation at the leading edge. An examination of the difference in pressure distributions to be discussed next can be studied to see why this might be the case.

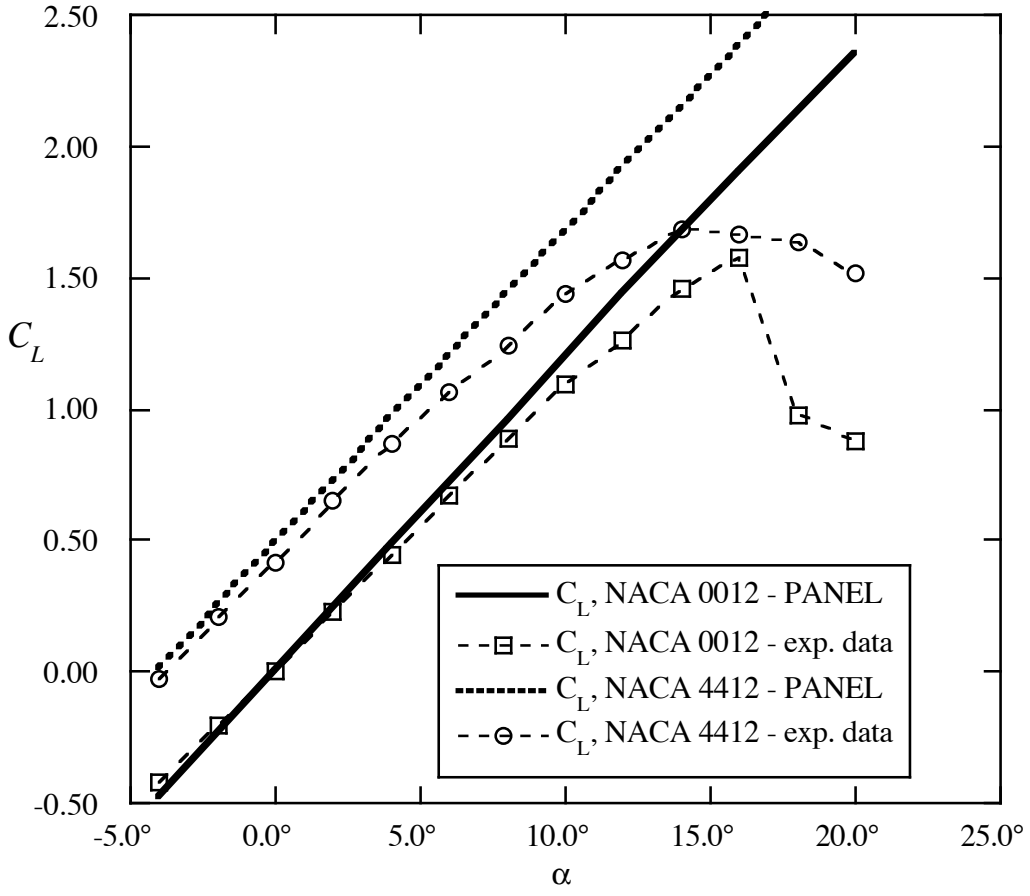

Figure 6-7. Comparison of **PANEL** lift predictions with experimental data, (Ref. 20).

The pitching moment characteristics are also important. Figure 6-8 provides a comparison of the **PANEL** pitching moment predictions (about the quarter chord point) with experimental data. In this case the calculations indicate that the computed location of the aerodynamic center, $dC_m / dC_L = 0$, is not exactly at the quarter chord, although the experimental data is very close to this value. The uncambered NACA 0012 data shows nearly zero pitching moment until flow separation starts to occur. The cambered airfoil shows a significant pitching moment, and a trend due to viscous effects that is exactly opposite the computed prediction.

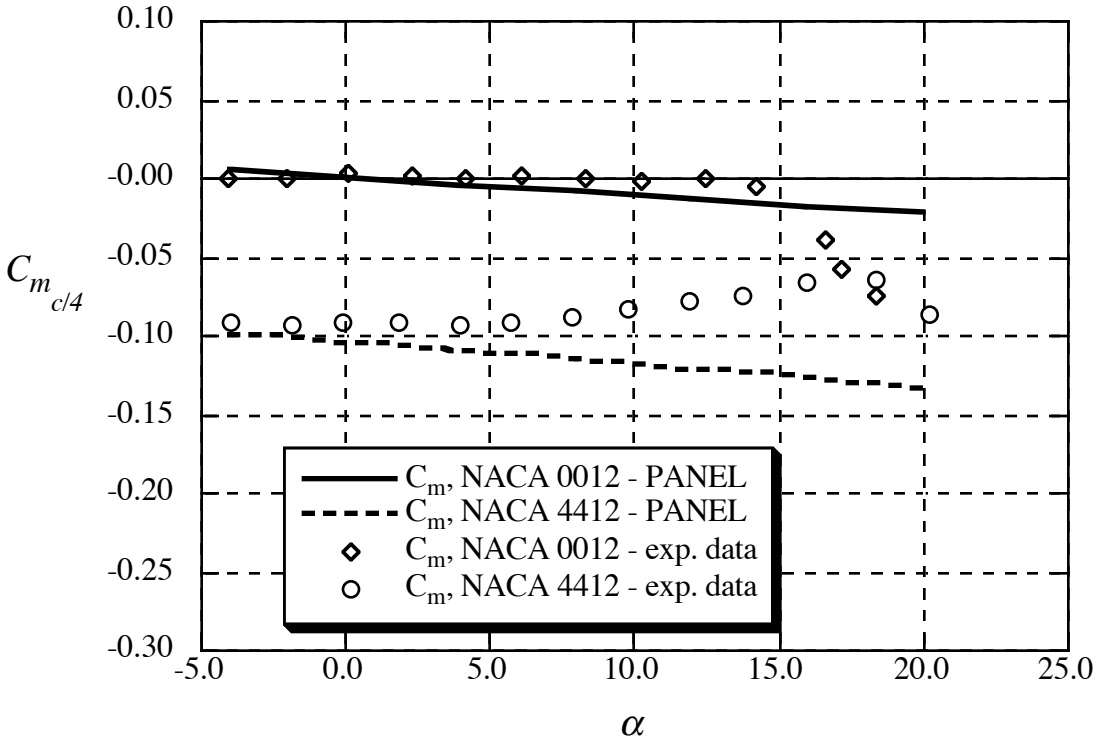

Figure 6-8. Comparison of **PANEL** moment predictions with experimental data, (Ref.20).

We do not compare the drag prediction from **PANEL** with experimental data. In two-dimensional incompressible inviscid flow the drag is supposed to be zero. In the actual case, drag arises from skin friction effects, further additional form drag due to the small change of pressure on the body due to the boundary layer (which primarily prevents full pressure recovery at the trailing edge), and drag due to increasing viscous effects with increasing angle of attack. A well-designed airfoil will have a drag value very nearly equal to the skin friction and nearly invariant with incidence until the maximum lift coefficient is approached.

Even though we don't include predictions, we include the experimental drag polars corresponding to the lift and moment cases given above. Figure 6-9 contains the experimental data showing the effect of camber on the drag polar, using the 0012 and 4412 cases. Note that the

cambered airfoil has a higher drag than the uncambered airfoil at low lift coefficients, but starts to show an advantage above about C_L of 0.3, and is clearly superior at around a C_L of 0.6 to 0.9. The minimum drag is always higher for the cambered airfoil. The aerodynamicist has to decide on the appropriate amount of camber for each application. Note also that the results given here are for old airfoils. The opportunity exists to design modern airfoils that operate over a wide range of lift coefficients without incurring drag penalties. The appeal of variable camber, either through leading edge and trailing device deflection schedules or smart structure "morphing" is also evident.

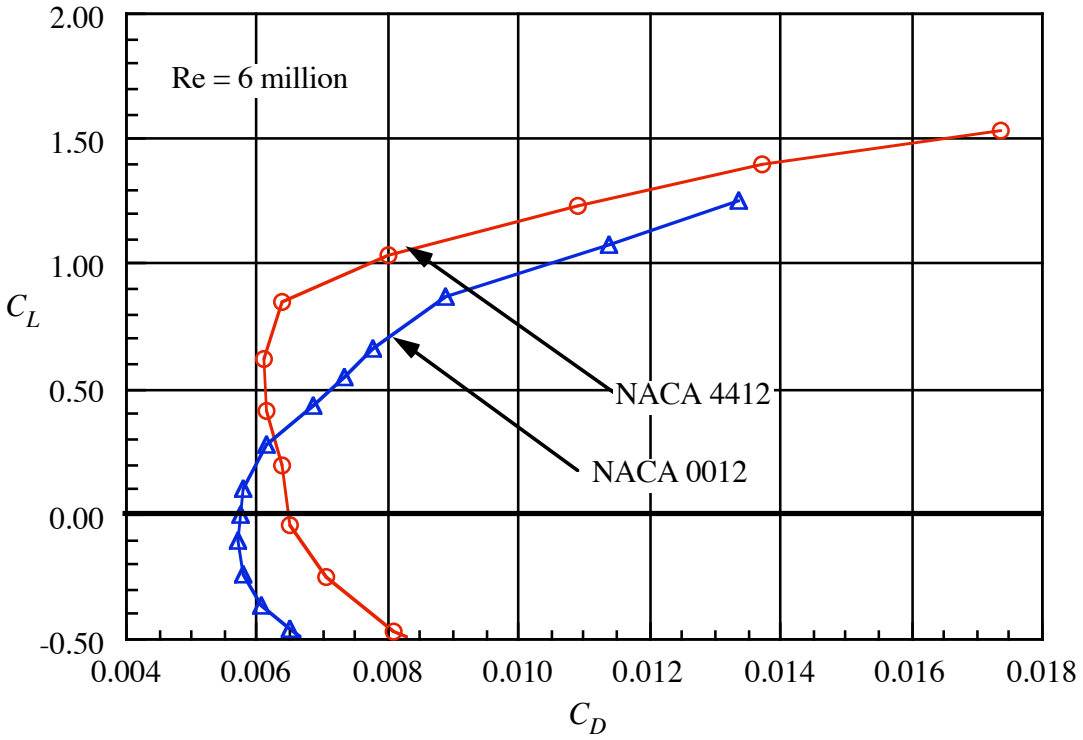

Figure 6-9 Experimental drag polars for the NACA 0012 and 4412 airfoils (Ref. 20)

In addition to force and moment comparisons, we need to compare the pressure distributions predicted with **PANEL** to experimental data. Figure 6-10 provides one example. The NACA 4412 experimental pressure distribution is compared to **PANEL** predictions. The agreement is generally very good. The primary disagreement is at the trailing edge. Here viscous effects act to prevent the recovery of the experimental pressure to the levels predicted by the inviscid solution.

Finally, panel methods often have trouble with accuracy at the trailing edge of thin airfoils with cusped trailing edges, where the included angle at the trailing edge is zero. The 6-series airfoils are an example. This problem is demonstrated in *Applied Computational Aerodynamics*, Chap. 4. In those cases, **PANEL** may give poor results locally near the trailing edge.

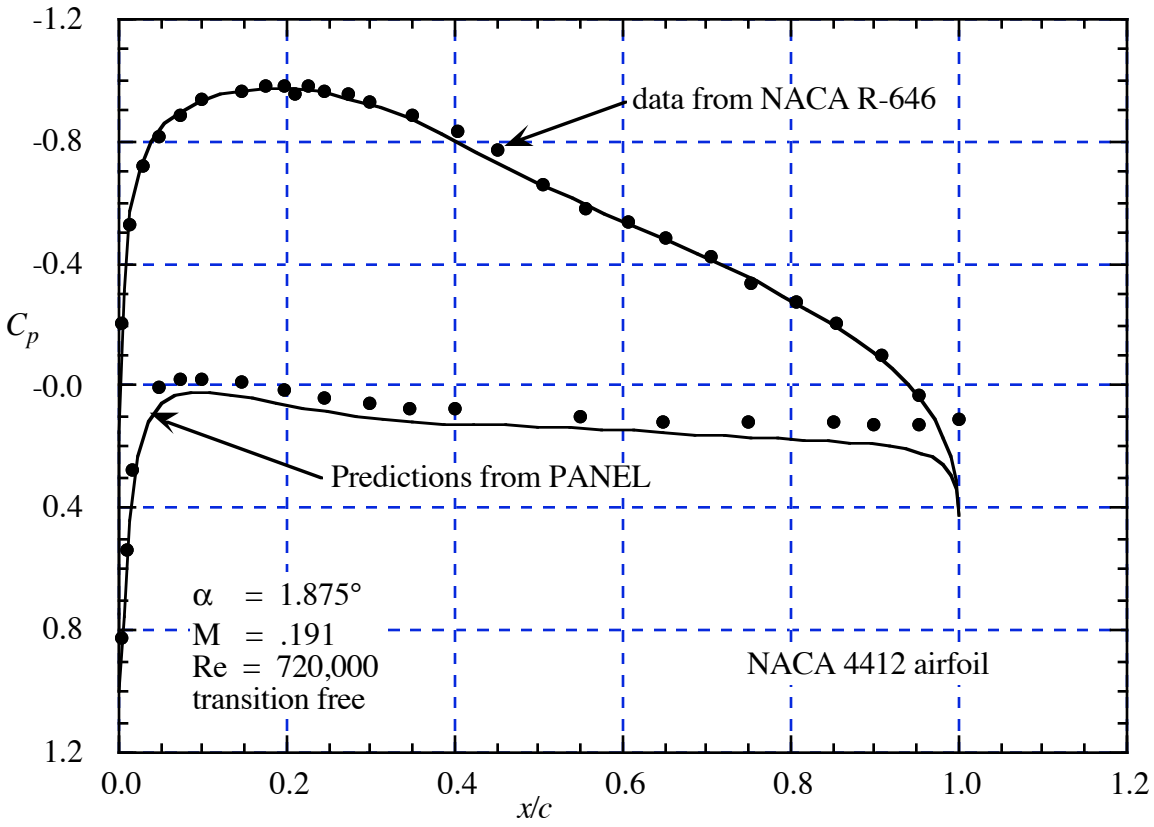

Figure 6-10. Comparison of pressure distribution from **PANEL** with data.

Note that the 6-series airfoils were very difficult to use on operational aircraft because of the thin cusped trailing edges. Subsequently, the 6A-series airfoils were introduced to remedy the problem. These airfoils have larger trailing edge angles (approximately the same as the 4-digit series), and were made up of nearly straight (or flat) surfaces over the last 20% of the airfoil. Most applications of 6-series airfoils today actually use the modified 6A-series thickness distribution.

6.2.2 Subsonic Airfoil Aerodynamics

> *"…mankind can be divided into two great classes: those who take airfoil selection seriously and those who don't."*
>
> Peter Garrison, *Flying Magazine*, September 2002

In this section we will try to demonstrate how airfoil selection is related to subsonic aerodynamics. Using **PANEL** we have a means of easily examining pressure distributions, and forces and moments, for different airfoil shapes. We present a discussion of airfoil characteristics using an inviscid analysis. We illustrate key areas to examine when studying airfoil pressure distributions using the NACA 0012 airfoil at 4° angle of attack as typical in Figure 6-11.

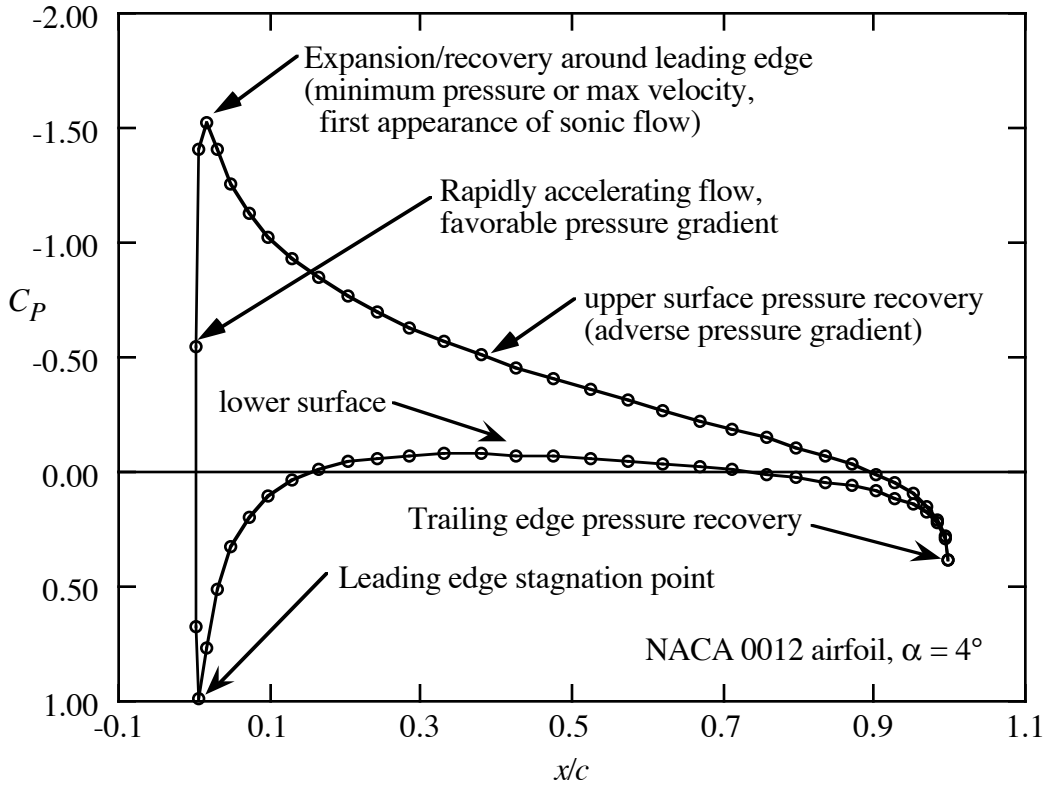

Figure 6-11. Key areas of interest when examining airfoil pressure distributions.

Several aspects of the pressure distribution shown in Figure 6-11 should be discussed. First, note that for subsonic 2D flow, the stagnation pressure coefficient should be one. As the Mach number increases, the value will increase slightly. For swept wings, the stagnation point pressure coefficient will be less then one. The rapid flow acceleration near the leading edge, and subsequent recompression can suggest the possibility of flow separation. The abruptness depends on the airfoil shape close to the leading edge. Bigger leading edge radii soften this flow feature, as well as reducing sensitivity to angle of attack. Finally, observe the value of the pressure coefficient at the trailing edge. If the C_p seen in data or a viscous calculation is greater than about 0.20, the flow can be assumed to be attached, a desirable feature.

Remember that we are making an incompressible, inviscid analysis when we are using program **PANEL**. Thus, in this section we examine the basic characteristics of airfoils from that point of view. We will examine viscous and compressibility effects subsequently. However, the best way to understand airfoil characteristics from an engineering standpoint is to examine the inviscid properties, and then consider changes in properties due to the effects of viscosity. Controlling the pressure distribution through selection of the geometry, the aerodynamicist controls, or suppresses, adverse viscous effects. In my view the mental concept of the flow best starts as a flowfield driven by the pressure distribution that would exist if there were no viscous effects. The airfoil characteristics then change by the "relieving" effects of viscosity, where flow separation or

boundary layer thickening reduces the degree of pressure recovery that would occur otherwise. For efficient airfoils the viscous effects should be small at normal operating conditions.

Overview of Airfoil Characteristics: Good and Bad

In this section we illustrate the connection between the airfoil geometry and the airfoil pressure distribution. We identify and discuss ways to control the inviscid pressure distribution by changing the airfoil geometry. An aerodynamicist controls viscous effects by controlling the pressure distribution. Further discussion and examples providing insight into aerodynamic design are available in the excellent book by Jones.[21] A book that captures much of the experience of the original designers of the NACA airfoils was written by aeronautical pioneer E.P. Warner.[22]

Drag: We discussed the requirement that drag should be zero* for this *two-dimensional* inviscid incompressible irrotational prediction method when we studied the accuracy of the method in the previous section. At this point we infer possible drag and adverse viscous effects by examining the effects of airfoil geometry and angle of attack on the pressure distribution.

Lift: Thin airfoil theory predicts that the lift curve slope should be 2π, and thick airfoil theory says that it should be slightly greater than 2π, with 2π being the limit for zero thickness. You can easily determine how close program **PANEL** comes to this value. These tests should give you confidence that the code is operating correctly. The other key parameter is α_{ZL}, the angle at which the airfoil produces zero lift (a related value is C_{L0}, the value of C_L at $\alpha = 0.0$).

Moment: Thin airfoil theory predicts that subsonic airfoils have their aerodynamic centers at the quarter chord for attached flow. The value of C_{m0} depends on the camber. We have seen in Figure 6-8 that the computed aerodynamic center is not precisely located at the quarter chord. However, the slope of the moment curve in Figure 6-8 corresponds to an aerodynamic center location of x/c = 0.2597, which is reasonably close to 0.2500.

Multi-element airfoils are also an important class of airfoils. However, their performance is so closely connected to the effects of viscosity that the discussion of those airfoils is deferred until we address viscous effects at the first order in the chapter on high-lift aerodynamics.

* Three-dimensional panel methods can estimate the induced drag.

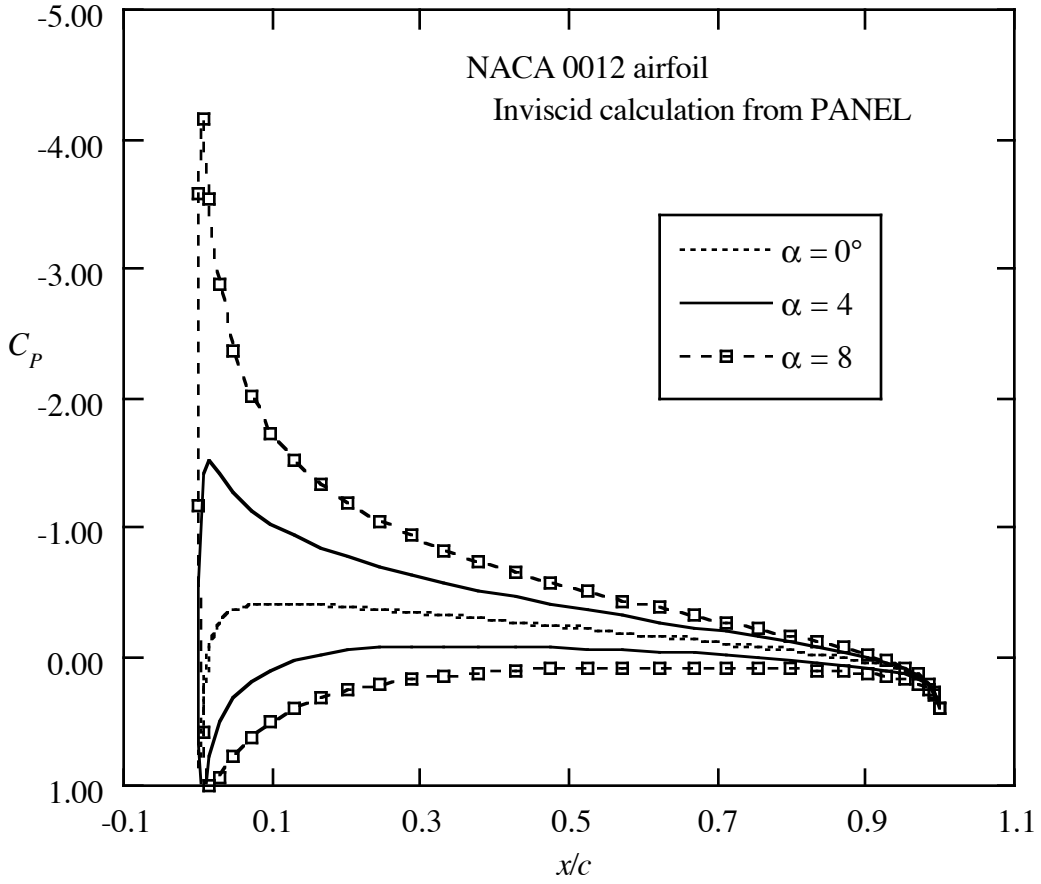

Figure 6-12. Effect of angle of attack on the pressure distribution.

The starting place for understanding airfoil characteristics is an examination of the angle of attack effects on an uncambered airfoil. Figure 6-12 presents this effect for the NACA 0012 airfoil. Here we see the progression from the symmetric zero angle of attack result. The $\alpha = 0°$ case produces a mild expansion around the leading edge followed by a monotonic recovery to the trailing edge pressure. As the angle of attack increases the pressure begins to expand rapidly around the leading edge, reaching a very low pressure, and resulting in an increasingly steep pressure recovery at the leading edge.

The next effect of interest is thickness. Figure 6-13 presents airfoil shapes for NACA 4 digit sections of 6, 12, and 18 percent thickness to chord ratio. The associated basic pressure distributions at zero angle of attack are shown in Figure 6-14. Clearly the thicker airfoil produces a larger disturbance, and hence a lower minimum pressure. However, the 18 percent thick airfoil produces a slightly milder expansion around the leading edge. The recompression near the trailing edge is also milder, and extends further upstream than the thinner airfoils.

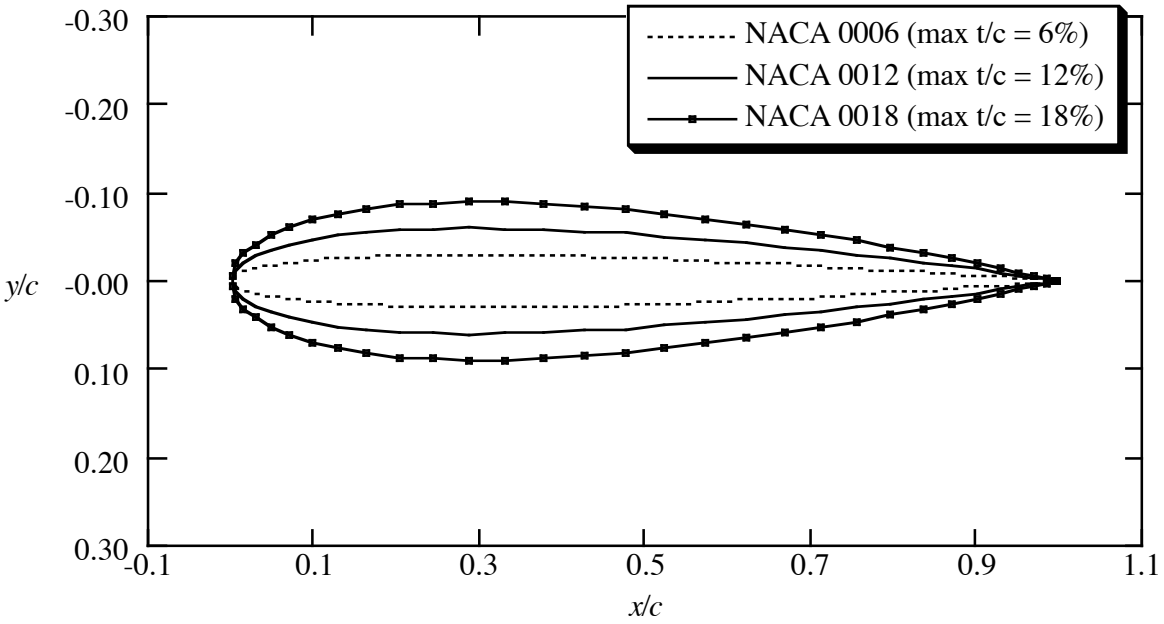

Figure 6-13. Comparison of NACA 4-digit airfoils of 6, 12, and 18% thicknesses.

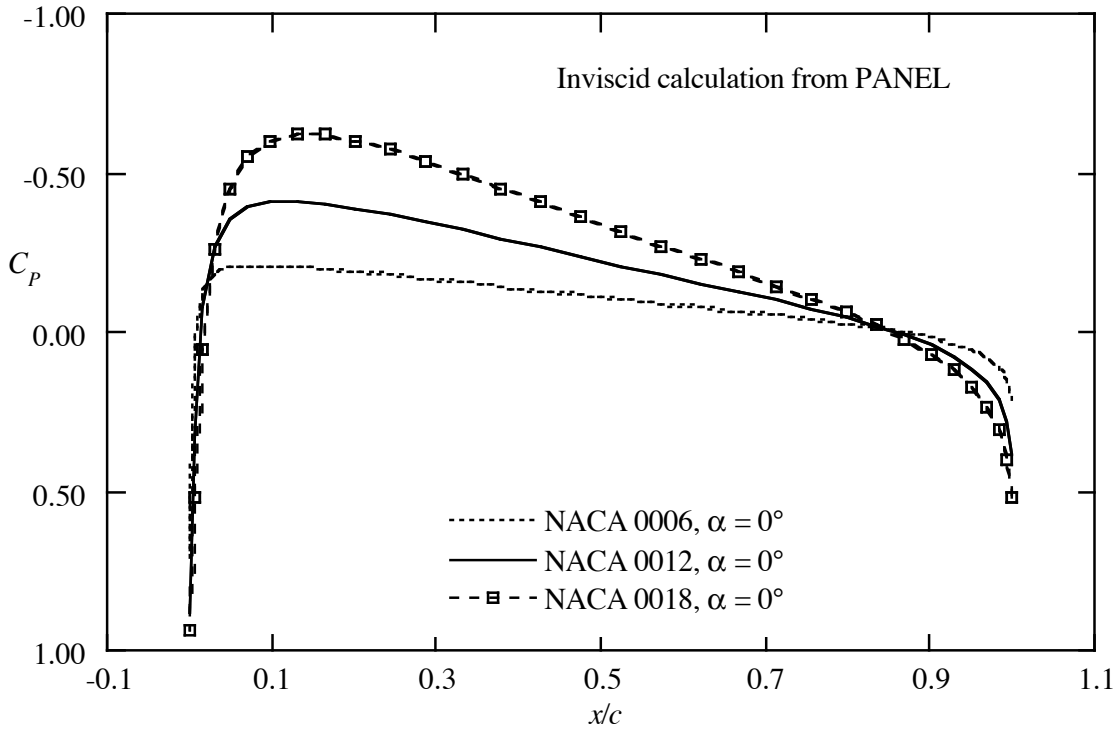

Figure 6-14. Effect of airfoil thickness on the pressure distribution at zero lift.

The effect of thickness in softening the expansion and recompression around the leading edge is even more evident at an angle of attack. Figure 6-15 shows this effect at a lift coefficient of 0.48. The thinnest airfoil shows a dramatic expansion/recompression due to the location of the stagnation

point below the leading edge point, requiring a rapid flow expansion around the leading edge that has a very small radius of curvature. The thicker airfoil results in a significantly milder expansion and subsequent recompression due to its large leading edge radius. Also note that the pressure distributions shift "upward" as the thickness increases. However the ΔC_p is nearly the same for each difference thickness, as predicted using the superposition of thickness, camber and angle of attack effects arising in thin airfoil theory.

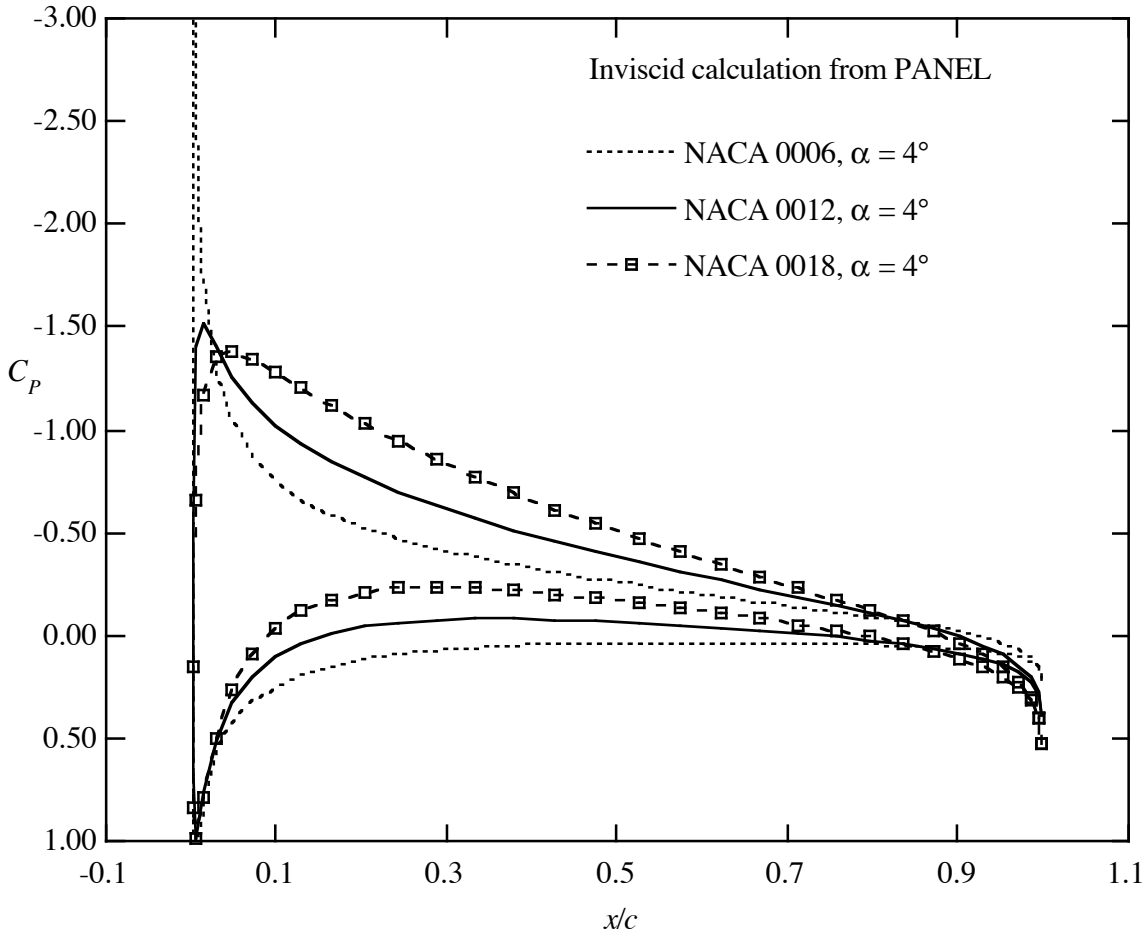

Figure 6-15. Effect of airfoil thickness on the pressure distribution at $C_L = 0.48$

The next effect to examine is camber. Figure 6-16 compares the shapes of the NACA 0012 and 4412 airfoils. The pressure distributions on the cambered airfoil for two different angles of attack are shown in Figure 6-17. Note the role of camber in obtaining lift without producing the rapid leading edge expansion and following recompression that we've seen before. This reduces the possibility of leading edge separation. Instead, the lift is distributed along the airfoil.

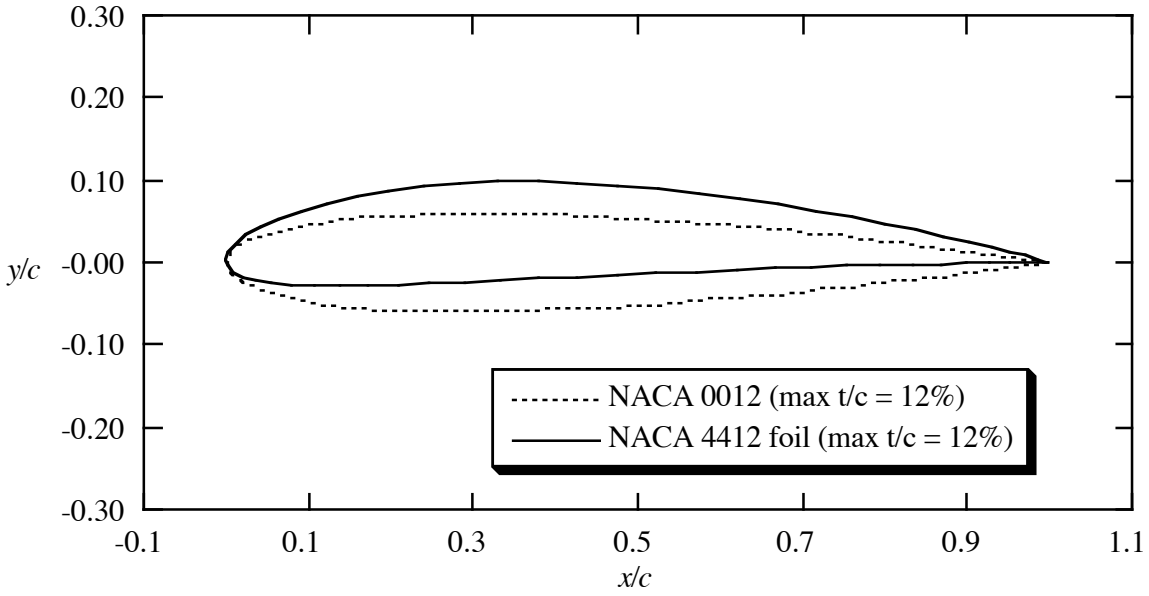

Figure 6-16. Comparison of uncambered and cambered NACA 4-digit airfoils.

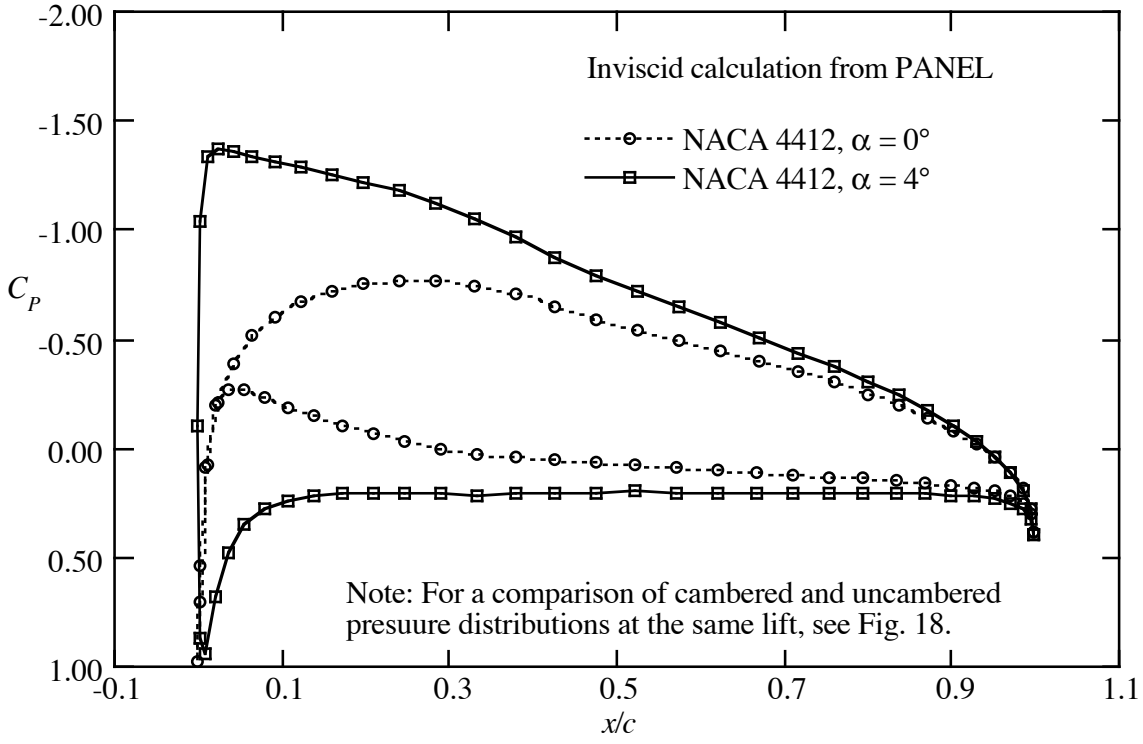

Figure 6-17. Effect of angle of attack on cambered airfoil pressure distributions at low lift.

A comparison of the NACA 0012 and NACA 4412 airfoil pressure distributions at the same lift coefficient is presented for several values of lift in Figures 6-18, 6-19 and 6-20. As the lift increases, the camber effects start to be overcome by the angle of attack effects, and the dramatic effects of camber are diminished until at a lift coefficient of 1.43 the pressure distributions start to appear to be very similar.

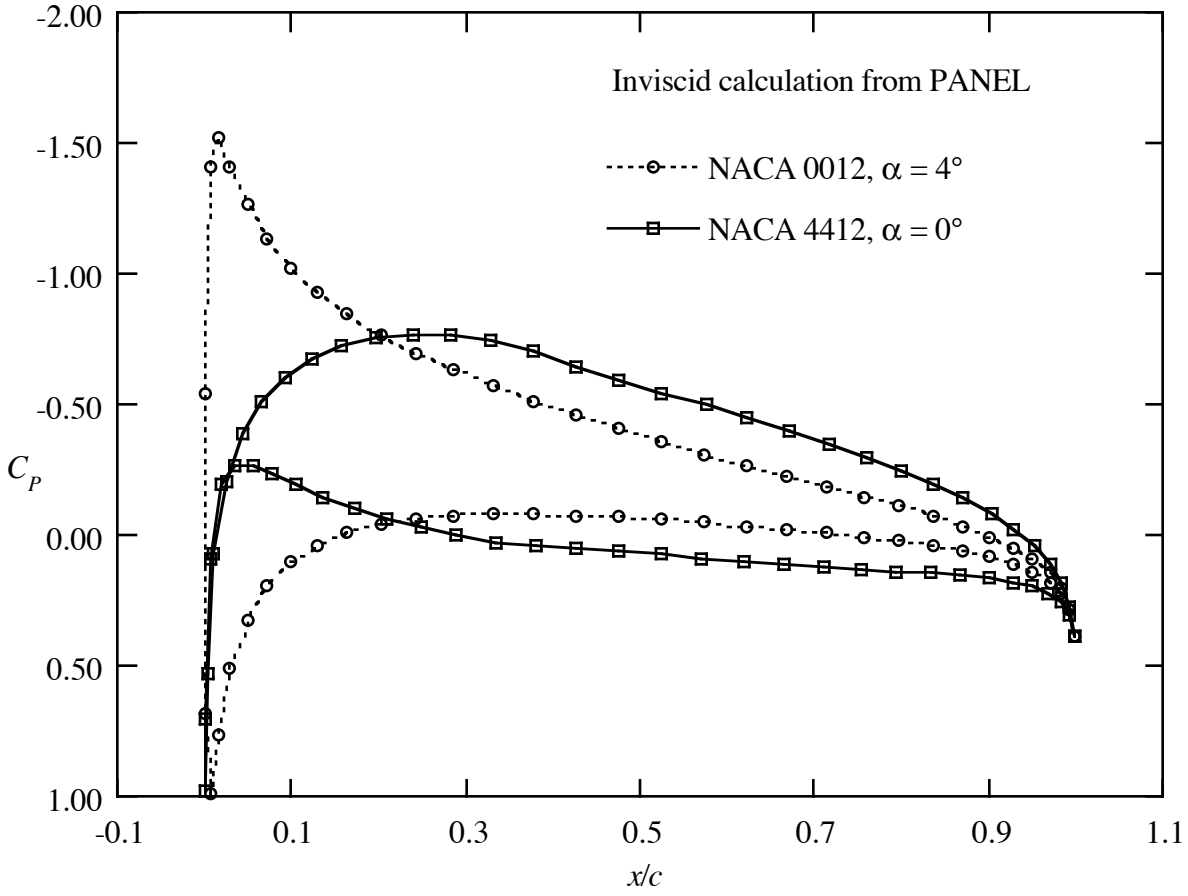

Figure 6-18. Camber effects on airfoil pressure distributions at $C_L = 0.48$.

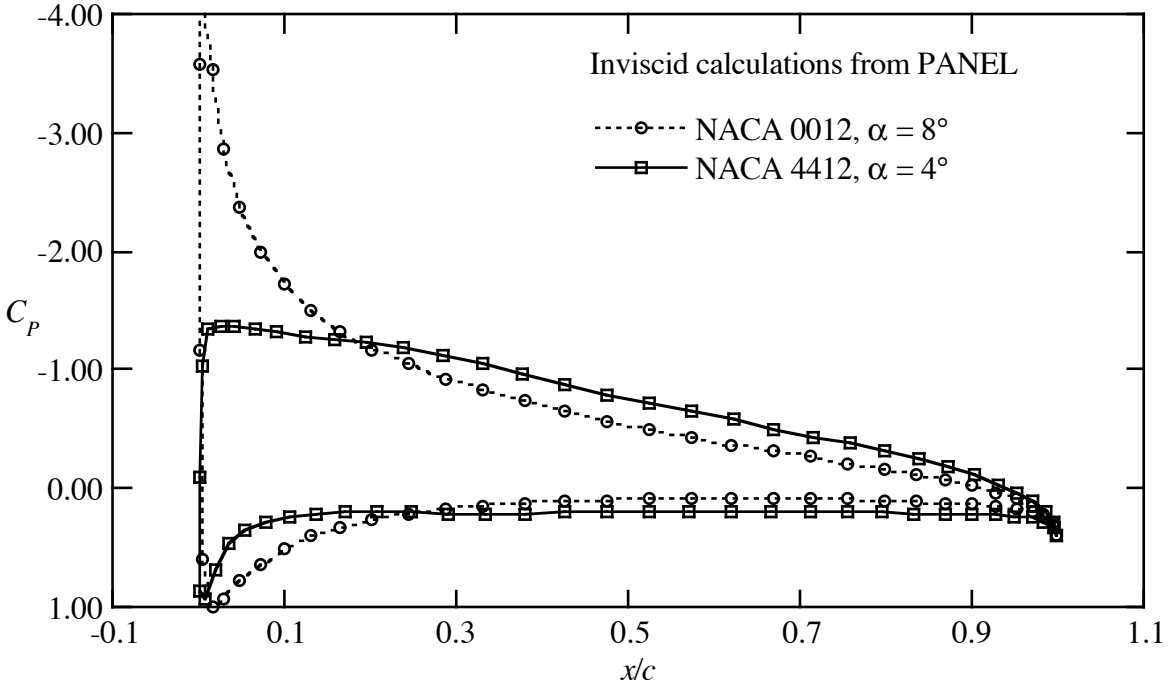

Figure 6-19. Camber effects airfoil pressure distributions at $C_L = 0.96$.

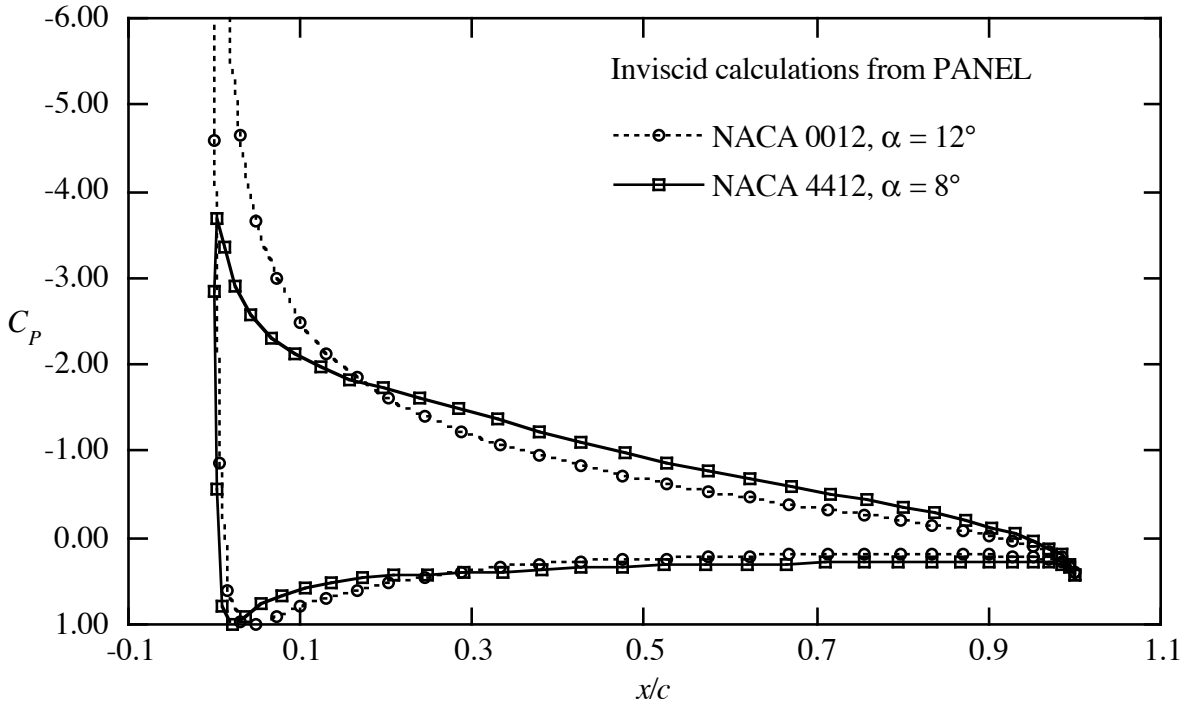

Figure 6-20. Camber effects airfoil pressure distributions at $C_L = 1.43$.

Finally, we examine the effect of extreme aft camber, which was part of the design strategy of Whitcomb when the so-called NASA supercritical airfoils were developed. This effect can be simulated using the NACA 6712 airfoil, as shown in Figure 6-21. The resulting pressure distribution is given in Figure 6-22. Note that the aft camber "opens up" the pressure distribution near the trailing edge. Two adverse properties of this type of pressure distribution are the large zero lift pitching moment and the delayed and then rapid pressure recovery on the upper surface. This type of pressure recovery is a very poor way to try to achieve a significant pressure recovery because the boundary layer will separate early. Whitcomb's design work primarily improved the pressure recovery curve.

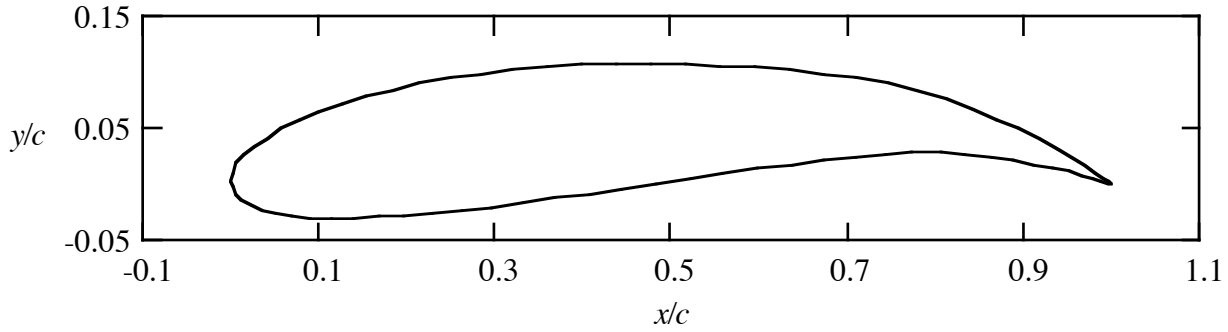

Figure 6-21. Highly aft cambered NACA airfoil, an NACA 6712.

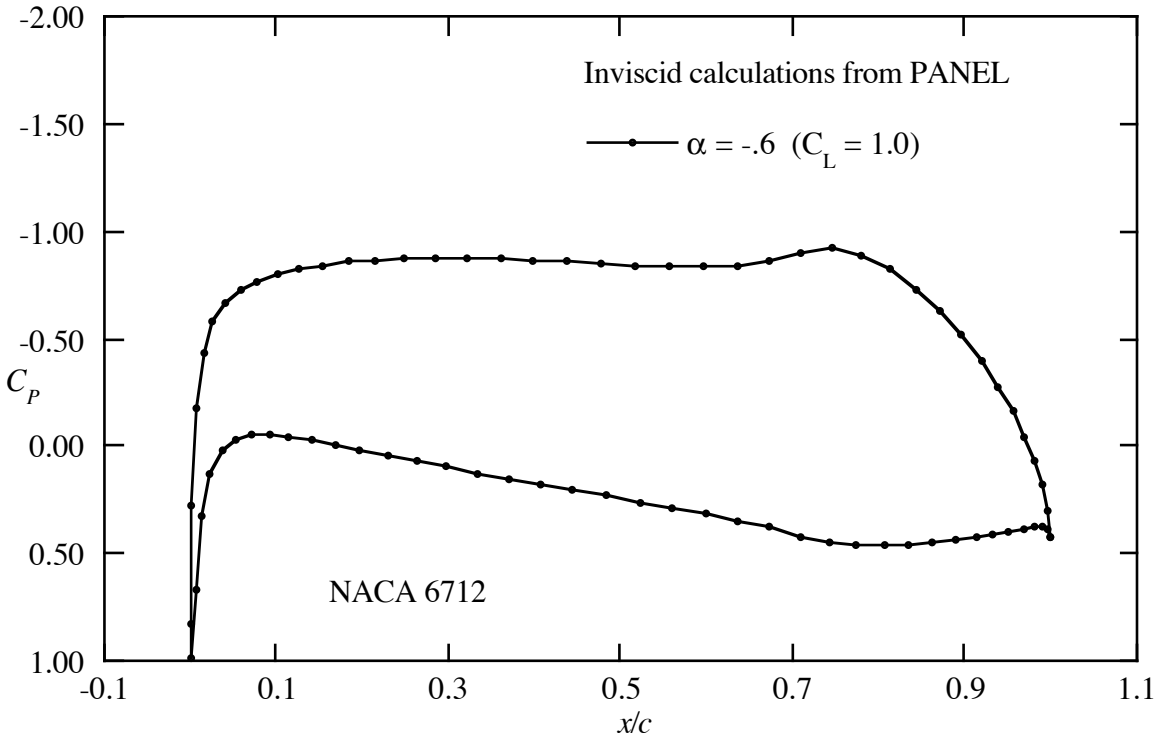

Figure 6-22. Example of the use of aft camber to "open up" the pressure distribution near the trailing edge.

The airfoils used to demonstrate geometry effects on pressure distributions above use parametric geometry definition formulas developed in the 1930s. More modern airfoils are available to the aerodynamicist. Unfortunately, to obtain improved performance, the designs were developed without the use of simple geometric definitions, and are available only as tables of coordinates. One modern airfoil that extends some of the previous shapes to obtain a high performance airfoil is the GA(W)-1 airfoil.[23] This 17% thick airfoil designed by NASA's Richard Whitcomb provides improved maximum lift and stall characteristics compared to previous NACA airfoils. Figure 6-23 shows the airfoil shape, and Figure 6-24 shows the pressure distribution.

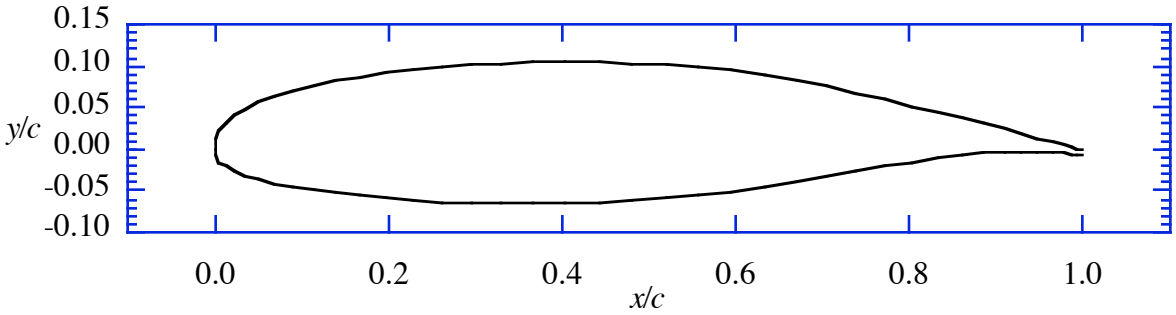

Figure 6-23. GA(W)-1 airfoil, also known as NASA LS(1)-0417.

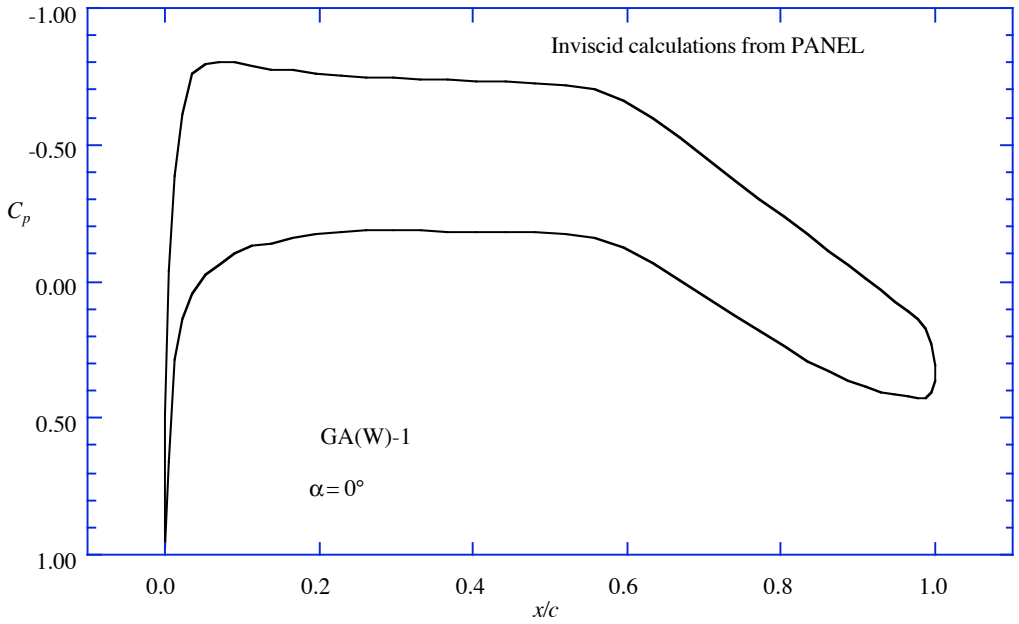

Figure 6-24. Pressure distribution at zero angle of attack of the GA(W)-1.

Notice that in this case the upper surface pressure distribution reaches a constant pressure plateau, and then has a moderate pressure recovery. Aft camber is used to obtain lift on the lower surface and "open up" the airfoil pressure distribution near the trailing edge in a manner suggested

previously in Figure 6-22. The area of aft camber on the lower surface is known as the "cove" region. If the camber is too extreme here the adverse pressure gradient will be too steep, and the flow will separate on the lower surface before it separates on the upper surface. This type of pressure distribution has a significantly more negative C_{m0} than conventional airfoil sections.

Airfoil Design

Having surveyed the broad effects of various shape changes on the airfoil pressure distribution, we now make a few comments on airfoil design. At subsonic speeds, the issues are low parasite (skin friction) drag at low lift coefficients, basic airfoil pitching moment, and maximum lift. To get low skin friction drag, a significant portion of the boundary layer should be laminar. This is possible for relatively small airplanes (say up to regional jet size) and surfaces with small sweep angles. Modern composite manufacturing techniques, which can produce extremely smooth surfaces are an enabling technology. Generally this is achieved passively by delaying the onset of any adverse pressure gradients until aft on the airfoil. Various combinations of active (boundary layer suction) and passive laminar flow control are possible. A recent survey of laminar flow technology is available,[24] as well as a chapter in an AIAA Progress in Astronautics and Aeronautics book.[25] The aft camber illustrated above provides extra lift, but with a possible penalty of a large C_{m0}. Finally, high maximum lift coefficients are desirable, and ways of obtaining high lift are discussed in Chapter 8, Aerodynamics of High Lift. Essentially achieving high lift depends on using a pressure distribution that maximizes the load carrying capacity of the boundary layer. Note that most current airfoil design activity also addresses transonic flow effects, where the shock strength for a specified lift coefficient should be minimized.

Effects of Shape Changes on Pressure Distributions: So far the examples have demonstrated global effects of camber and thickness. To develop an understanding of the typical effects of adding local modifications to the airfoil surface, an exercise at the end of this chapter provides a framework for the reader to carry out an investigation to understand the effects of local shaping on the airfoil characteristics. I have had good luck using a smooth "cubic bump" to modify surfaces. The key with those types of airfoil shape modifications is to distribute the bump over a large portion of the airfoil, say one half to nearly the entire chord, with relatively low amplitude changes. Short "bumps" lead to poor off-design performance. It is also worthwhile to investigate the very powerful effects that small deflections of the trailing edge can produce. This reveals the power of the Kutta condition, and alerts the aerodynamicist to the basis for the importance of the viscous effects at the trailing edge.

Computational experimentation is extremely educational when implemented in an interactive computer program, where the aerodynamicist can make shape changes with a mouse and see the

effect on the pressure distribution immediately. An outstanding code that does this has been created by Ilan Kroo.[26] It is known as *PANDA*.

Shape for a specified pressure distribution: There is another way that aerodynamicists view the design problem. The local modification approach described above is useful to make minor changes in airfoil pressure distributions. Often the aerodynamic designer wants to find the geometric shape corresponding to a prescribed pressure distribution. This problem is known as the "inverse problem." It is more difficult than the analysis problem. In fact, it is possible to prescribe a pressure distribution for which no geometry exists. Even if the geometry exists, it may not be acceptable from a structural standpoint. For two-dimensional incompressible flow it is possible to obtain conditions on the surface velocity distribution that ensure that a closed airfoil shape exists. Excellent discussions of this problem have been given by Volpe[27] and Sloof.[28] A two-dimensional panel method has been developed by Bristow.[29] Numerical optimization can also be used to find the shape corresponding to a prescribed pressure distribution.[30]

Camber line design and program DesCam

Most of the discussion above corresponds to the analysis problem, and we've given only a very brief discussion of the inverse problem for subsonic flows. However, the airfoil camber line for a prescribed loading, ΔC_p, can be found easily with vortex lattice methods, which are used often in three-dimensional flows as described in the next section. Here the chord load, is specified and the camber shape required to produce the prescribed load is found. In this section we provide an example. Program **DesCam** is used to make the calculation using a slight variation of the **VLM** method known as the quasi-vortex lattice method developed by Prof. Edward Lan of the University of Kansas.[10] His method uses a mathematically based selection of vortex and control point placements instead of the 1/4 - 3/4 rule typically used in **VLM** methods. One interesting aspect of the inverse problem is that it is a direct solution, and does not require the solution of a system of equations. Instead, the shape is computed from a straightforward algebraic calculation to find camber line slopes. Once the slopes are known, they are integrated to obtain the camber line. The details of the method are given in Chapter 6 of *Applied Computational Aerodynamics*.

Figure 6-25 provides an example. We compare the results from **DesCam** with the analytic formula given in Appendix A, Geometry for Aerodynamicists, for the NACA 6 Series mean line with $a = 0.4$. Notice that the camber scale is greatly enlarged to demonstrate the excellent comparison. Even though the chord load is constructed by prescribing two straight-line segments, the resulting required camber line is highly curved over the forward portion of the airfoil. Note also that thin airfoil theory allows only two possible values for the pressure differential at the leading edge, zero or infinity. A finite load at the leading edge is not possible. A close examination of the camber line shape required to produce a finite load reveals a singularity. The camber slope is

infinite at the leading edge. This feature is much easier to study using the analytic solution, as given in the Appendix. This type of approach to obtaining the desired pressure loading can easily be extended to three dimensions.

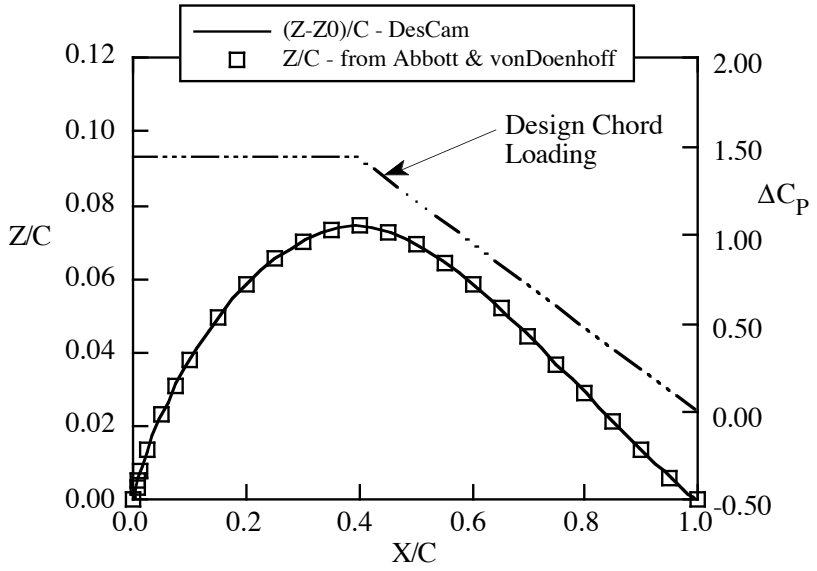

Figure 6-25. Example and verification of camber design using **DesCam**.

Finally, to learn more about subsonic airfoil design, read the papers by Liebeck[31] and Drela[32] in the AIAA Progress in Aeronautics and Astronautics series volume *Applied Computational Aerodynamics*.

6.2.3 Airfoil Selection

Having covered some of the basic ideas of airfoil aerodynamics, we conclude our airfoil discussion by summarizing the issues associated with choosing an airfoil for a particular application. Even though we've discussed airfoils before planforms, the logical progression is to start with the mission of the airplane (requirements), then select the appropriate planform(s), and finally the airfoil(s). You should match the planform and the airfoil.

The basic issues are the cruise performance (cruise C_L) and the field performance (max lift). When considering trade studies for various planform and airfoil combinations, recall that the objective is to minimize drag, not drag coefficient. So the aerodynamicist should be evaluating $D/q = S_{wng}C_D$.

In cruise, the C_L for L/D_{max} should be found from the planform selection and the estimated C_{D0}. In general, the higher the aspect ratio (AR) the higher the C_L for L/D_{max} The choice of a predominantly laminar flow or turbulent flow airfoil should be addressed at this point. In particular, the laminar flow airfoils tend to operate in a narrowly defined range of lift coefficients to achieve the

design performance (drag). Note also that the wing C_L and airfoil section C_l's may be different. The airfoil C_l requirement should be used to select the camber required. In addition, transonic cruise speeds require special consideration (see the next chapter) and the 2D airfoil problem for an airfoil on a swept wing differs from just defining a streamwise cut for an airfoil on the wing. The relation between the airfoil problem and the swept wing planform is given later in this chapter. In general, the thickness to chord ratio (t/c) should be as large as possible to allow the wing structural weight to be low and provide internal volume.

Field performance starts with the requirement for the airplane to meet a specified stall or approach speed. This translates to a required C_{Lmax}. The conflict in requirements between efficient cruise (small wing) and low landing speed (big wing) means that most airplanes will have some type of high lift system, ranging from a simple flap to triple-slotted flap systems described in Chapter 8. Either a large leading edge radius is selected or a separate leading edge device is used to assist in obtaining the required lift. The high lift system should be as simple as possible to reduce manufacturing and maintenance cost.

Tail sections: For a vertical tail the section should be symmetric. For the horizontal tail the section is often symmetric. Low drag 6A-Series airfoils are often selected for tail surfaces, but have poor values for C_{Lmax}. The NACA 4 Digit sections have higher values of C_{Lmax}, but more zero lift drag. If the horizontal tail may be required to generate large downloads, a cambered airfoil may be used. This is more likely to occur when the airplane has a very powerful high-lift system. Note that the B-52s have vortex generators on the bottom surface of the horizontal tail to allow the tail to achieve the downforce required to trim the plane in takeoff and landing.

Finally, some help is available in choosing an airfoil. Gil Crouse has developed a software package called Airfoil Optimizer. [33]This program allows the user to specify design requirements, and the program will suggest an airfoil based on a large library of airfoils. This type of procedure falls under the category of an "expert system." Peter Garrison devoted a column to this package along with an excellent discussion of airfoil selection issues in his *Flying* magazine column Technicalities in 2002.

6.3 Wings

6.3.1 Use and Accuracy of the VLM Method

Before describing the aerodynamics of wings, examples will be provided of the typical use and accuracy of vortex lattice methods. Complete details are available in Chapter 6 of Applied Computational Aerodynamics. The vortex lattice layout is clear for most wings and wing-tail or wing-canard configurations. The method can be used for wing-body cases by simply specifying the projected planform of the entire configuration as a flat lifting surface made up of a number of straight-line segments. The exact origin of this somewhat surprising approach is unknown. The success of this approach is illustrated in examples given below.

To get good, consistent , reliable results, some simple rules for panel layout should be followed. This requires that a few common rules of thumb be used in selecting the planform break points: *i)* the number of line segments should be minimized, *ii)* breakpoints should line up streamwise* on front and rear portions of each planform, and should line up between planforms, *iii)* streamwise tips should be used, *iv)* small spanwise distances should be avoided by making edges streamwise if they are actually very highly swept, and *v)* trailing vortices from forward surfaces cannot hit the control point of an aft surface. Figure 6-26 illustrates these requirements.

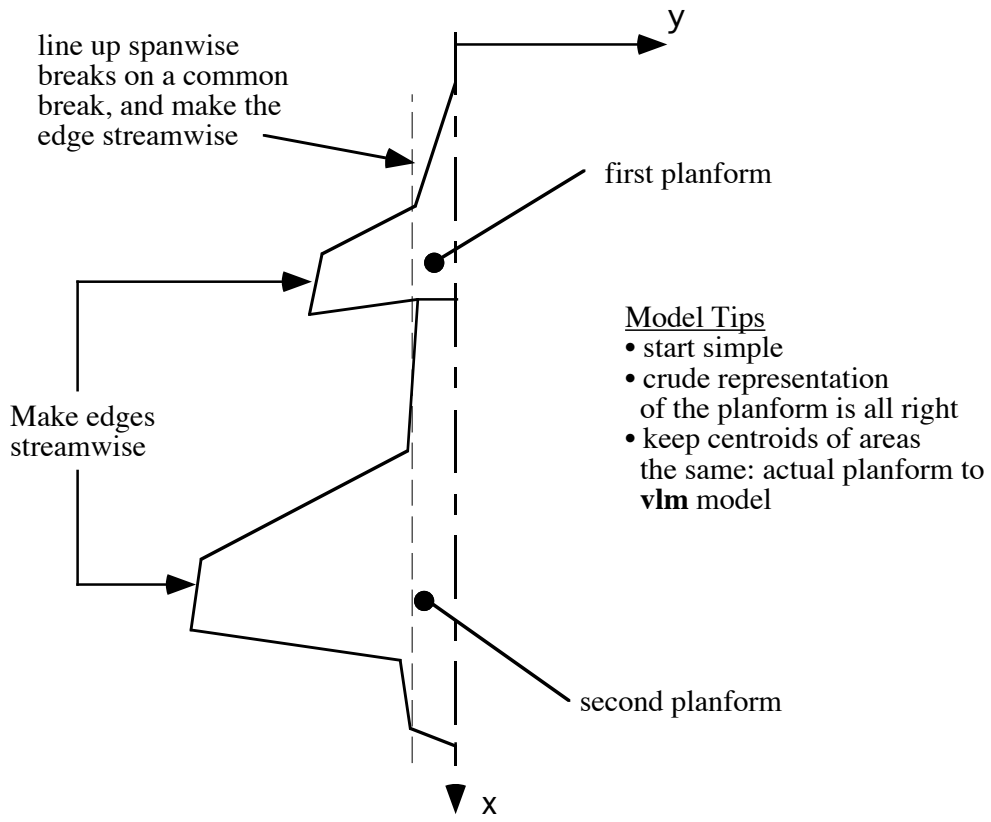

Figure 6-26. Example of a **VLM** model of an aircraft configuration. Note that one side of a symmetrical planform is shown.

* "Streamwise" means parallel to the freestream. In this coordinate system it means that *y* is a constant.

To illustrate typical results that can be expected from vortex lattice methods we provide some examples from a study by John Koegler[34]. It illustrates the range of uses for the **VLM** method. Koegler, studied the prediction accuracy of several methods for fighter airplanes. In addition to the vortex lattice method, he also used the PAN AIR and Woodward II panel methods (see Chapter 4 of *Applied Computational Aerodynamics* for a description of panel methods). He compared his predictions with the three-surface F-15, which became known as the STOL/Maneuver demonstrator, and the F-18. These configurations are illustrated in Figure 6-27.

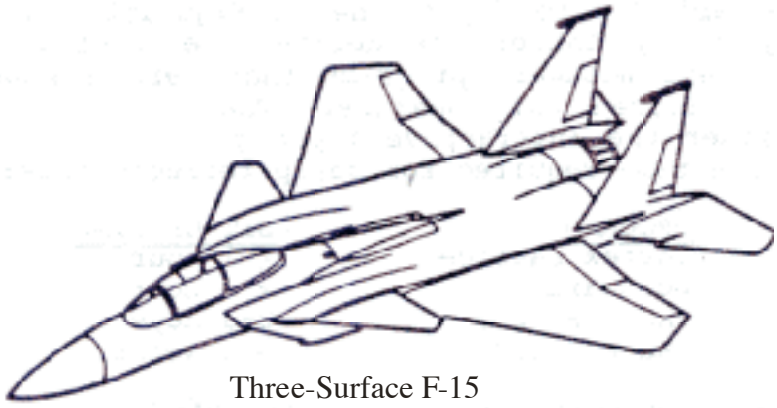

Three-Surface F-15

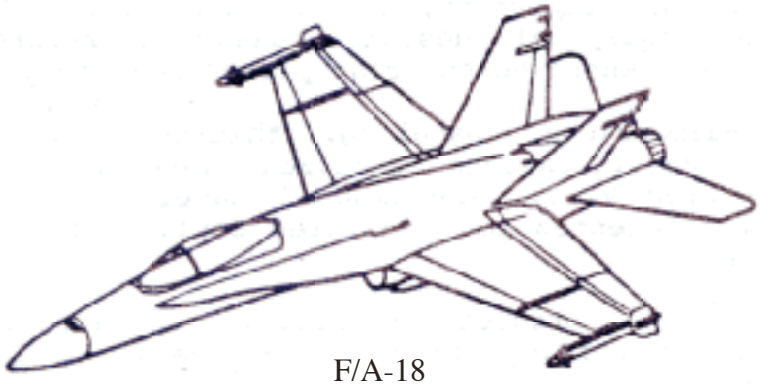

F/A-18

Figure 6-27. Configurations used by McDonnell Aircraft to study **VLM** method accuracy (Reference 34).

As with the panel method calculations for airfoils, before making the actual calculations, a study of the number of horseshoe vortices required to obtain good results must be made. The effects of the number of panels and the way they are distributed is presented in Figure 6-28 for the F/A-18 configuration shown in Figure 6-27. In this case the **VLM** method is seen to take between 130 to 220 panels to produce converged results. The change in neutral point is used because this is perhaps one of the most important uses of these methods in early aircraft design. For the vortex lattice method it appears important to use a large number of spanwise rows, and a relatively small number of chordwise panels (5 or 6 appear to be enough).

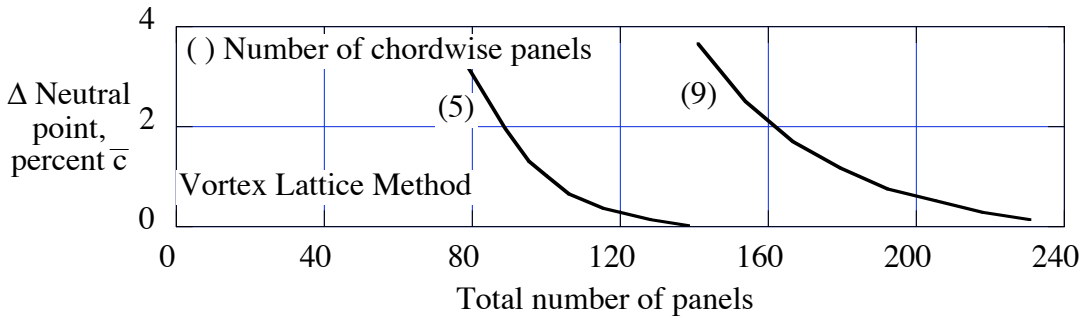

Figure 6-28. F/A-18 panel convergence study for a vortex lattice method (Ref. 34).

Considering the F-15 STOL/Maneuver demonstrator, the basic panel layout is given in Figure 6-29. Several computational models were studied. This shows how the aircraft was modeled as a flat planform, and the corner points of the projected configuration were used to represent the shape in the vortex lattice method. Note that in this case the rake of the wingtip was included in the computational model. In the vortex lattice model the configuration was divided into three separate planforms, with divisions at the wing root leading and trailing edges. On this configuration each surface was at a different height and, after some experimentation, the vertical distribution of surfaces shown in Figure 30 was found to provide the best agreement with wind tunnel data.

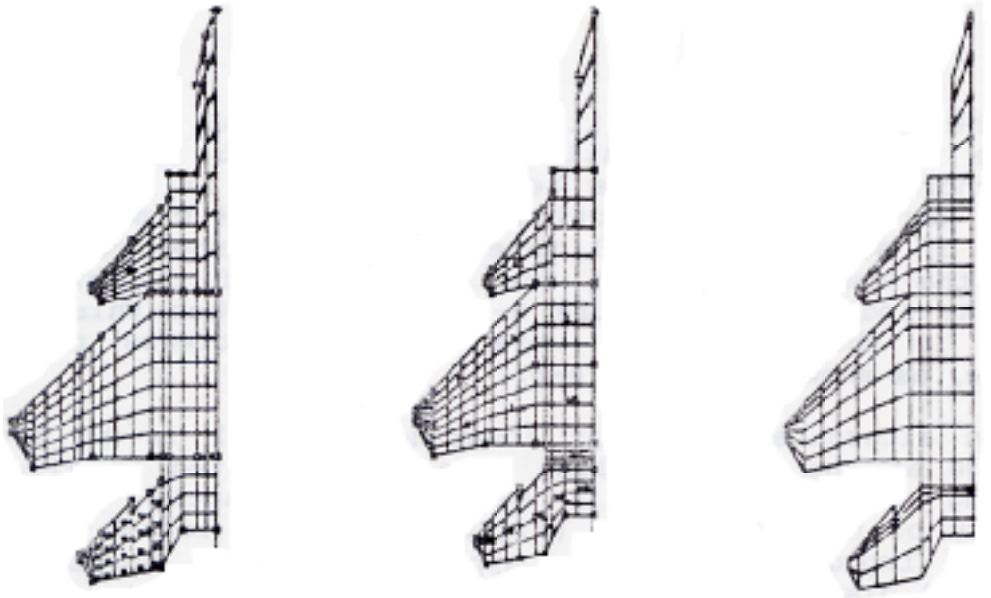

Figure 6-29. Panel models used for the three-surface F-15 (Ref.34).

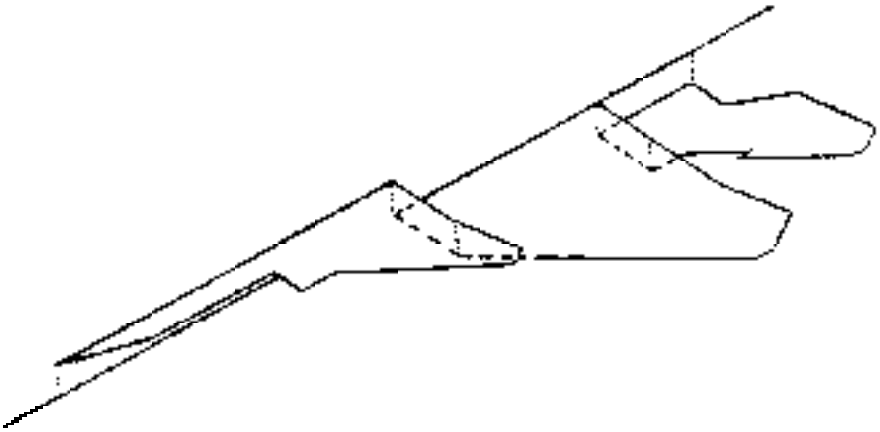

Figure 6-30. Canard and horizontal tail height representation (Ref. 34).

The results from these models are compared with wind tunnel data in Table 6-1. The vortex lattice method is seen to produce excellent agreement with the data for the neutral point location, and lift and moment curve slopes at Mach 0.2.

Subsonic Mach number effects are simulated in **VLM** methods by transforming the Prandtl-Glauert equation which describes the linearized subsonic flow to Laplace's Equation using the Göthert transformation. However, this is only approximately correct and the agreement with wind tunnel data is not as good at the transonic Mach number of 0.8. Nevertheless, the **VLM** method is as good as PAN AIR, which is a high-order panel method, used in this manner. The **VLM** method is not applicable at supersonic speeds. The wind tunnel data shows the shift in the neutral point between subsonic and supersonic flow. The Woodward method, as applied here, over predicted the shift with Mach number. Note that the three-surface configuration is neutral to slightly unstable subsonically, and becomes stable at supersonic speeds.

Figure 6-31 provides an example of the use of the **VLM** method to study the effects of moving the canard. Here, the wind tunnel test result is used to validate the method and to provide an "anchor" for the numerical study (it would have been useful to have to have an experimental point at -15 inches). This is typical of the use of the **VLM** method in aircraft design. When the canard is above the wing the neutral point is essentially independent of the canard height. However when the canard is below the wing the neutral point varies rapidly with canard height.

Table 1 Three-Surface F-15 Longitudinal Derivatives				
Data Source		Neutral Point (% mac)	$C_{m\alpha}$ (per deg.)	$C_{L\alpha}$ (per deg.)
M = 0.2	Wind Tunnel	15.70	0.00623	0.0670
	Vortex Lattice	15.42	0.00638	0.0666
	Woodward	14.18	0.00722	0.0667
	Pan Air	15.50	0.00627	0.0660
M = 0.8	Wind Tunnel	17.70	0.00584	0.0800
	Vortex Lattice	16.76	0.00618	0.0750
	Pan Air	15.30	0.00684	0.0705
M = 1.6	Wind Tunnel	40.80	-0.01040	0.0660
	Woodward	48.39	-0.01636	0.0700
from Ref. 34, Appendix by John Koegler				

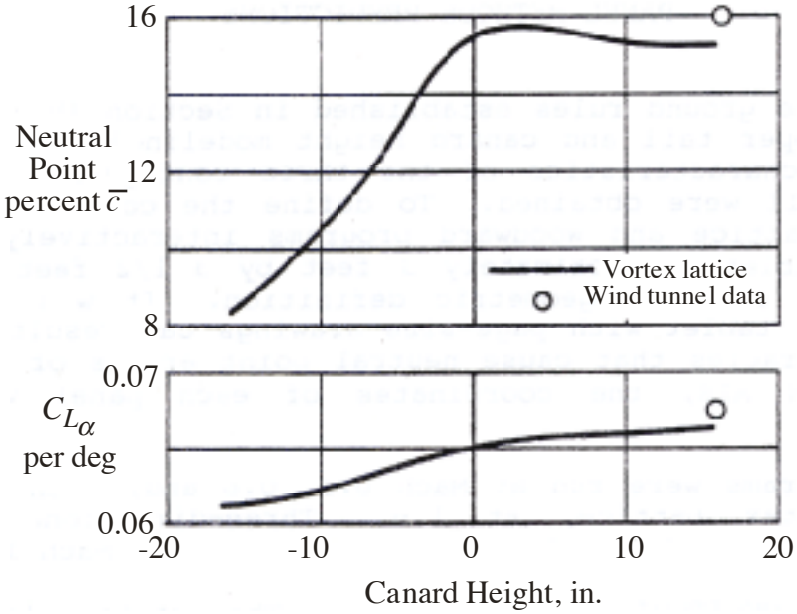

Figure 6-31. Effect of canard height variation on three-surface F-15 characteristics (Ref. 34).

Control effectiveness is also of interest in conceptual and preliminary design, and the **VLM** method can be used to provide estimates. Figure 6-32 provides an apparently accurate example of this capability for F-15 horizontal tail effectiveness. Both $C_{L\delta h}$ and $C_{m\delta h}$ are presented. The **VLM** estimate is within 10% accuracy at both Mach 0.2 and 0.8. However, the F-15 has an all-moving

horizontal tail to provide sufficient control power under both maneuvering and supersonic flight conditions. Thus the tail effectiveness presented here is effectively a measure of the accuracy of the prediction of wing lift and moment change with angle of attack in a non-uniform flowfield, rather than the effectiveness of a flap-type control surface. A flapped device such as a horizontal stabilizer and elevator combination will have significantly larger viscous effects, and the inviscid estimate from a vortex lattice or panel method (or any inviscid method) will overpredict the control effectiveness. This is shown next for an aileron.

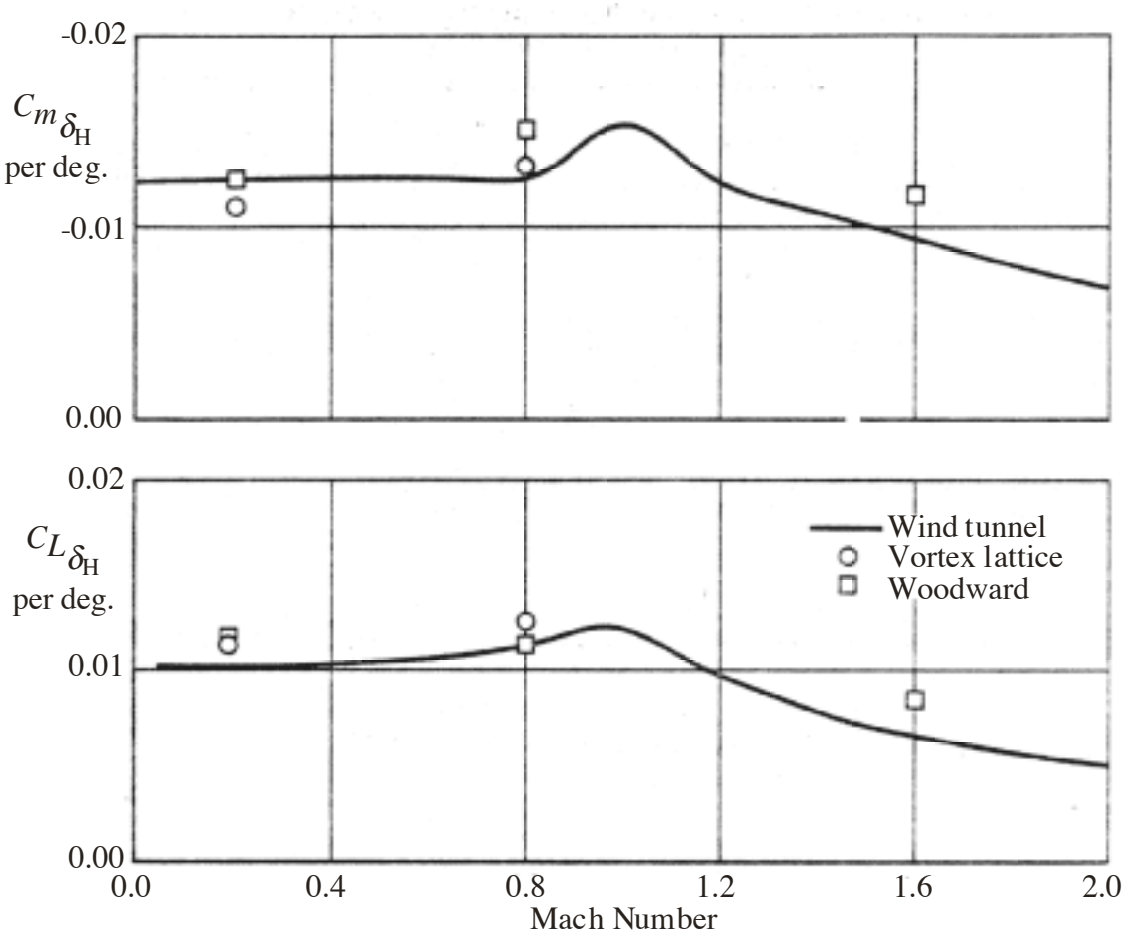

Figure 6-32. F-15 horizontal tail effectiveness (Ref. 34).

The aileron effectiveness for the F-15 presented in Figure 6-33 is more representative of classical elevator or flap effectiveness correlation between **VLM** estimates and experimental data. This figure presents the roll due to aileron deflection. In this case the device deflection is subject to significant viscous effects, and the figure shows that only a portion of the effectiveness predicted by the **VLM** method is realized in the actual data. The **VLM** method, or *any* method, should always be calibrated with experimental data close to the cases of interest to provide an indication of the

agreement between theory and experiment. In this case the actual results are found to be about 60% of the inviscid prediction at low speed.

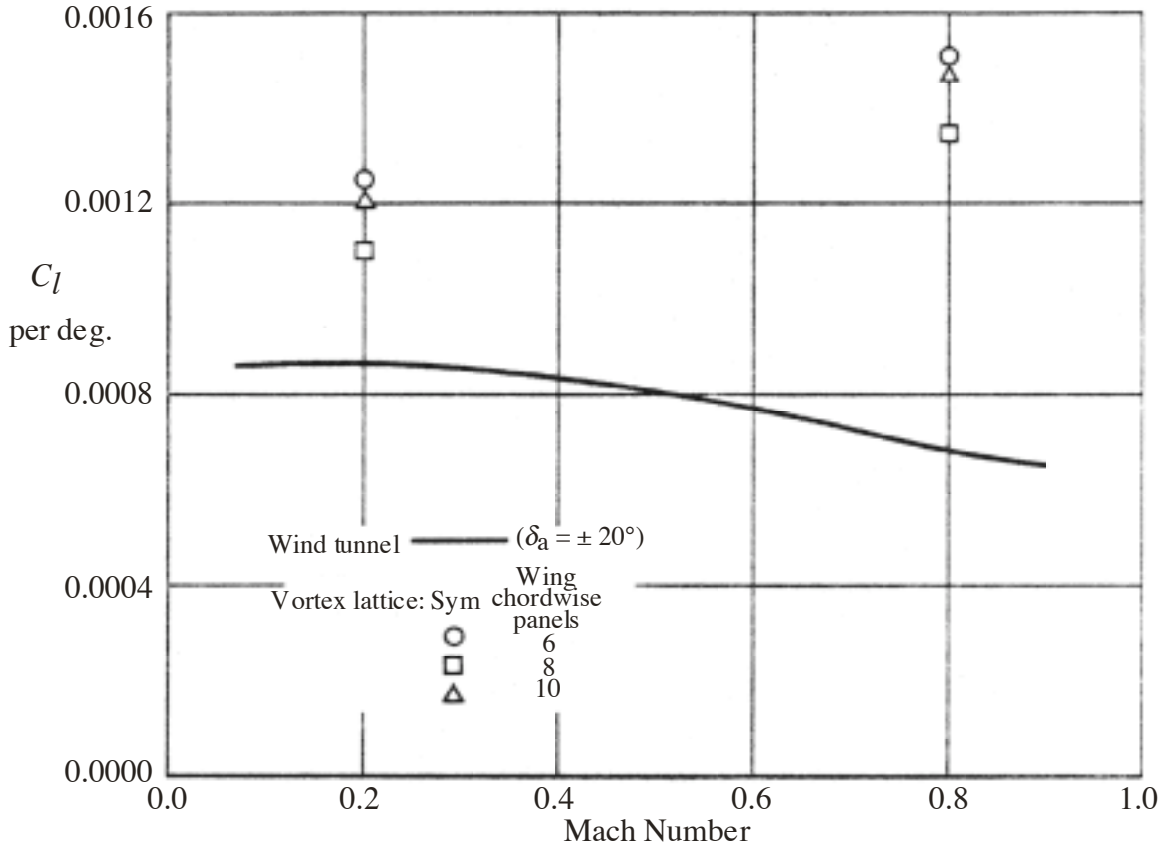

Figure 6-33. F-15 aileron effectiveness (Ref. 34).

6.3.2 Program VLMpc and the Warren 12 Test Case

This vortex lattice method can be used on personal computers. The version of the Lamar program described in NASA TN D-7921[7] fits easily into personal computers, and is available for student use (students typed this code in from the listing in the TN) as **VLMpc**. The code and input instructions are described on the software web site.

This code is still used in advanced design work, and can be used to investigate many ideas in wing aerodynamics. As shown above, results can be obtained and used before the large time consuming methods of CFD are used to examine a particular idea in detail.

This section defines one reference wing case that is typically used to check the accuracy of vortex lattice codes. It provides a ready check case for the evaluation of any new or modified code, as well as a check on the panel scheme layout. It is known as the Warren 12 planform, and is defined, together with the "official" characteristics from previous calculations, in Figure 6-34 below.

For the results given in the figure, the reference chord used in the moment calculation is the average chord (slightly nonstandard, normally the reference chord used is the mean aerodynamic

chord) and the moment reference point is located at the wing apex (which is also nonstandard). Any calculations made in starting to check your proficiency in making a **VLM** calculation should include this case.

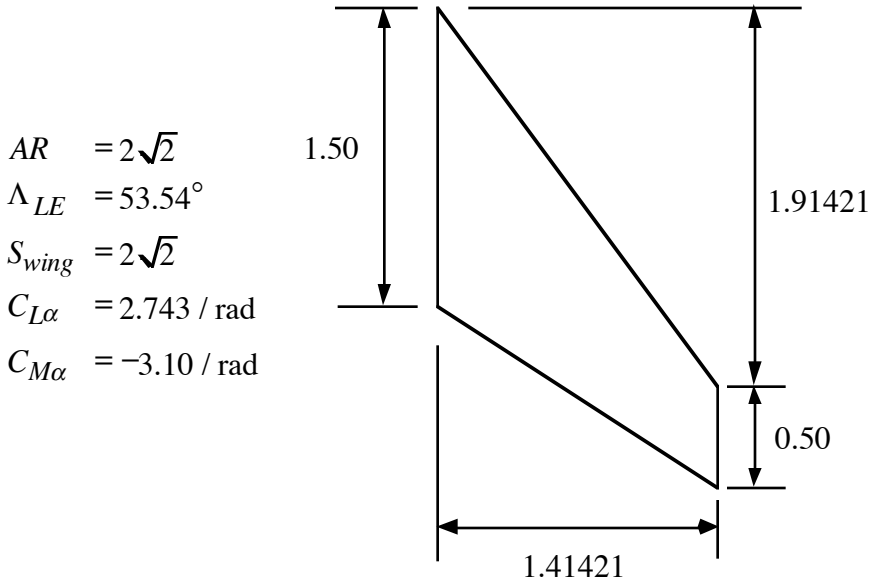

Warren-12 Planform

Figure 6-34. Definition and reference results for the Warren-12 wing.

6.3.3 Tornado and AVL

In addition to **VLMpc**, the MATLAB program **Tornado**, capable of handling very general geometries and flow conditions has been written by Tomas Melin at KTH in Stockholm[16]. Available on the web, this program has been used by many students, and may be replacing **VLMpc** as a standard. And even more recently **AVL** the code developed some years ago by Drela and Youngren has been placed in the public domain.[17]

6.3.4 Aerodynamics of High Aspect Ratio Wings

With a three-dimensional method available, we can examine the aerodynamics of wings. Most of the results presented in this section were computed using **VLMpc**. One key advantage of the vortex lattice method compared to lifting line theory is the ability to treat swept wings. Classical Prandtl lifting line theory is essentially correct for unswept wings, but is completely erroneous for swept wings. Aerodynamics of unswept wings are closely related to the airfoil characteristics of the airfoil used in the wing. This relationship is less direct for swept wings. Many of the most important wing planform-oriented characteristics of wings arise when the planforms are swept. Even though sweep is used primarily to reduce compressibility effects, the important aerodynamic features of swept wings can be illustrated at subsonic speeds using the **VLM** method.

Basic Ideas

Wings are designed to satisfy stability and handling characteristics requirements, while achieving low drag at the design conditions (usually cruise and sustained maneuver). They must also attain high maximum lift coefficients to meet field performance and maneuver requirements. Although these requirements might at first appear overwhelming, a small number of key characteristics can provide a basic physical understanding of the aerodynamics of wings.

Aerodynamic Center: The first key characteristic is the aerodynamic center of the wing, defined as location at which $dC_m/dC_L = 0$. The neutral point of the configuration is the aerodynamic center for the entire configuration. The **VLM** method was shown to provide accurate predictions of the neutral point for many configurations in the previous sections. The location of the neutral point is important in initial configuration layout to position the wing and any longitudinal stability and control surfaces at the proper location on the aircraft. Subsequently this information is fundamental in developing the control system. Wing planform shaping, as well as positioning, is used to control the location of the configuration neutral point.

Spanload: The next key consideration is the spanload distribution, cc_l/c_a, where c is the local chord, c_a is the average chord, and c_l is the local section lift coefficient. The spanload controls the location of the maximum section lift coefficient, the induced drag, and the magnitude of the wing root bending moment. The location and value of the maximum section lift coefficient provides a good initial estimate of where the wing will stall first.[*] If the wing stalls in front of a control surface, control will be poor at flight conditions just when control becomes very important. The shape of the spanload, together with the actual value of the wingspan, determines the value of the induced drag. For a specified span, the performance of the wing is evaluated by finding the value of the span efficiency factor, e, as described in the Drag notes. Finally, the wing root bending moment provides an indication of the structural loading requirements that the wing structure must be designed to accommodate. When considering the total system, the basic aerodynamic efficiency may be compromised to reduce structural wing weight. The shape of the spanload can be controlled through a combination of planform selection and wing twist. Typical twist distributions required to produce good wing characteristics are presented below.

The simplest example of planform shaping is the selection of wing aspect ratio, AR, wing taper, λ, and wing sweep, Λ. While the aerodynamicist would like to see high values of the aspect ratio, several considerations limit aspect ratio. Perhaps the most important limitation is the increase of wing structural weight with increasing aspect ratio. In addition, the lift coefficient required to maximize the benefits of high aspect ratio wings increases with the square root of the aspect ratio. Hence, airfoil performance limits can restrict the usefulness of high aspect ratios, especially for highly swept wings based on airfoil concepts. In recent years advances in both aerodynamics and

[*] For a trapezoidal wing with an elliptic spanload the maximum value of the local lift coefficient occurs at $\eta = 1 - \lambda$.

structures have allowed aircraft to be designed with higher aspect ratios and reduced sweep. Table 6-2 provides some key characteristics of transport wings designed to emphasize efficient cruise while meeting takeoff and landing requirements.

Taper: Several considerations are used in selecting the wing taper. For a straight untwisted, unswept wing, the minimum induced drag corresponds to a taper ratio of about 0.4. However, a tapered wing is more difficult and hence expensive to build than an untapered wing. Many general aviation aircraft wings are built with no taper (all ribs are the same, reducing fabrication cost, and the maximum section C_l occurs at the root, well away from the control surface, providing positive roll control at stall, a very good feature). To reduce structural weight, the wing should be highly tapered, with $\lambda < 0.4$. However, although highly tapered wings are desirable structurally, the section lift coefficient near the tip may become high. This consideration limits the amount of taper employed (current jet transports use taper ratios in the range of 0.2 to 0.3, as well as progressively increasing twist upward from the tip). In one other example, the Aero Commander 500 has an aspect ratio of 9.5 and a taper ratio of 0.5 (it also has -6.5° of twist and the quarter chord of the wing was swept forward 4°).

Table 6-2
Typical Planform Characteristics of Major Transport Aircraft

1st Flight	Aircraft	*W/S*	AR	$\Lambda_{c/4}$ °	λ
1957	B707-120	105.6	7.04	35.0	0.293
1958	DC-8-10	111.9	7.32	30.0	0.230
1963	B707-320C	110.0	7.06	35.0	0.250
1970	B747-200B	149.1	6.96	37.5	0.254
1970	L-1011	124.4	8.16	35.0	0.200
1972	DC-10-30	153.7	7.57	35.0	0.230
1972	A300 B2	107.9	7.78	28.0	0.230
1982	A310-100	132.8	8.80	28.0	0.260
1986	B767-300	115.1	7.99	31.5	0.182
1988	B747-400	149.9	7.61	37.5	0.240
1990	MD-11	166.9	7.57	35.0	0.230
1992	A330	119.0	9.30	29.7	0.192
1994	B777-200	118.3	8.68	31.6	0.172

data courtesy Nathan Kirschbaum

Sweep: Sweep is used primarily to delay the effects of compressibility and increase the drag divergence Mach number. The Mach number controlling these effects is approximately equal to the Mach number normal to the leading edge of the wing, $M_{\text{eff}} = M_\infty \cos\Lambda$. The treatise on swept

planforms by Küchemann is very helpful in understanding swept wing aerodynamics.[35] Aerodynamic performance is based on the wingspan, b. For a fixed span, the structural span increases with sweep, $b_s = b/\cos\Lambda$, resulting in a higher wing weight. Wing sweep also leads to aeroelastic problems. For aft swept wings flutter becomes an important consideration. If the wing is swept forward, divergence is a problem. Small changes in sweep can be used to control the aerodynamic center when it is not practical to adjust the wing position on the fuselage (the DC-3 is the most famous example of this approach).

To understand the effects of sweep, the Warren 12 wing is compared with wings of the same span and aspect ratio, but unswept and swept forward. The planforms are shown in Figure 6-35. The wing leading edge sweep of the aft swept wing becomes the trailing edge sweep of the forward swept wing. Figure 6-36 provides the spanload and section lift coefficient distributions from **VLMpc**. The spanload, cc_l / c_a, is given in Figure 6-36a, where, c is the local chord, c_l is the local lift coefficient, based on the local chord, and c_a is the average chord, S/b. Using this nomenclature, the area under the curve is the total wing lift coefficient. Note that sweeping the wing aft increases the spanload outboard, while sweeping the wing forward reduces the spanload outboard. This follows directly from a consideration of the vortex lattice model of the wing. In both cases, the portion of the wing aft on the planform is operating in the induced upwash flowfield of the wing ahead of it, resulting in an increased spanload. Figure 6-36b shows the corresponding value of the local lift coefficient. Here the effect of sweep is more apparent. The forward swept wing naturally results in a spanload with a nearly constant lift coefficient. This means that a comparatively higher wing lift coefficient can be achieved before the wing stall begins. The program **LIDRAG** can be used to compare the span e's associated with these spanloads (an exercise for the reader).

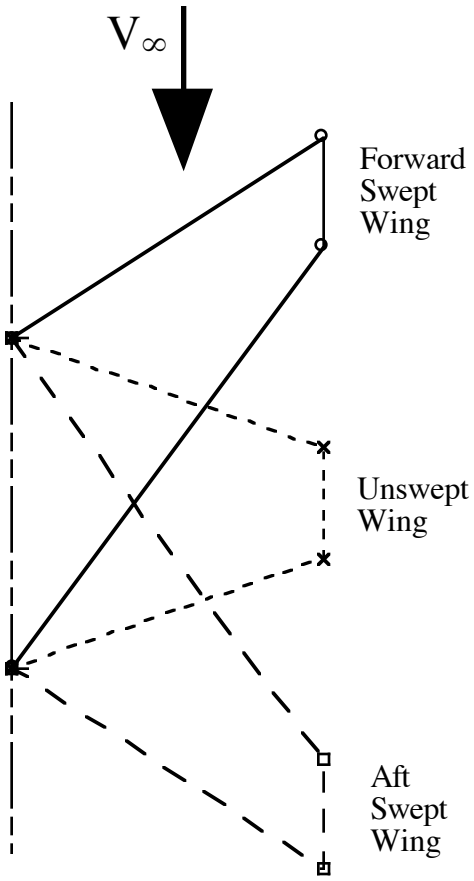

Figure 6-35. Comparison of forward, unswept, and aft swept wing planforms, AR = 2.8.

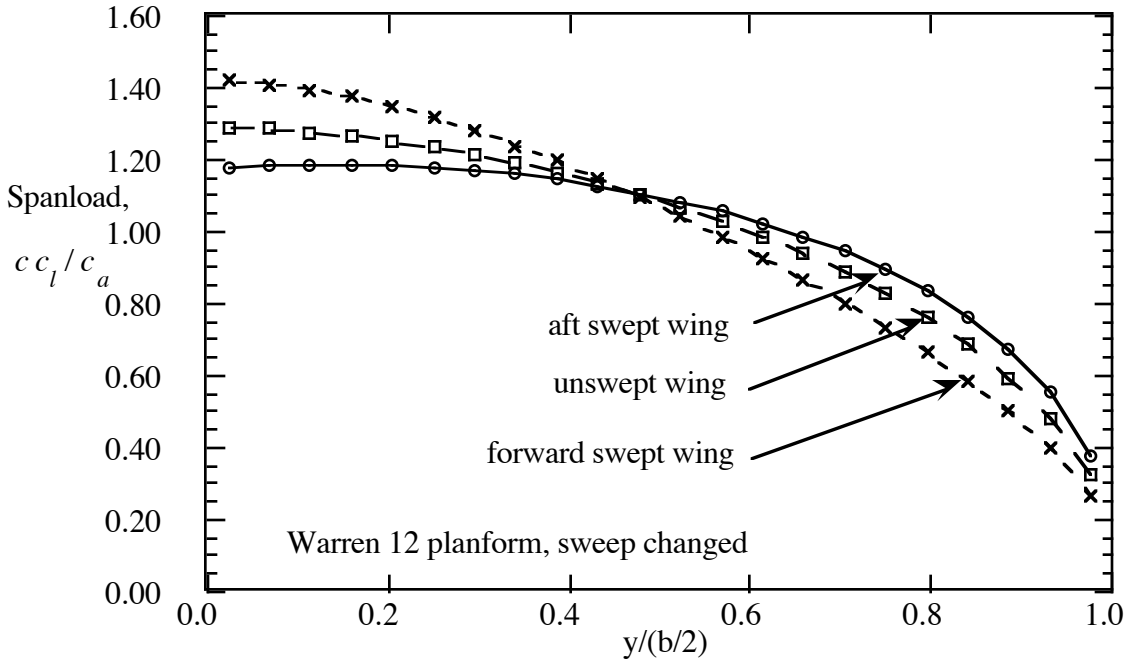

a) comparison of spanloads

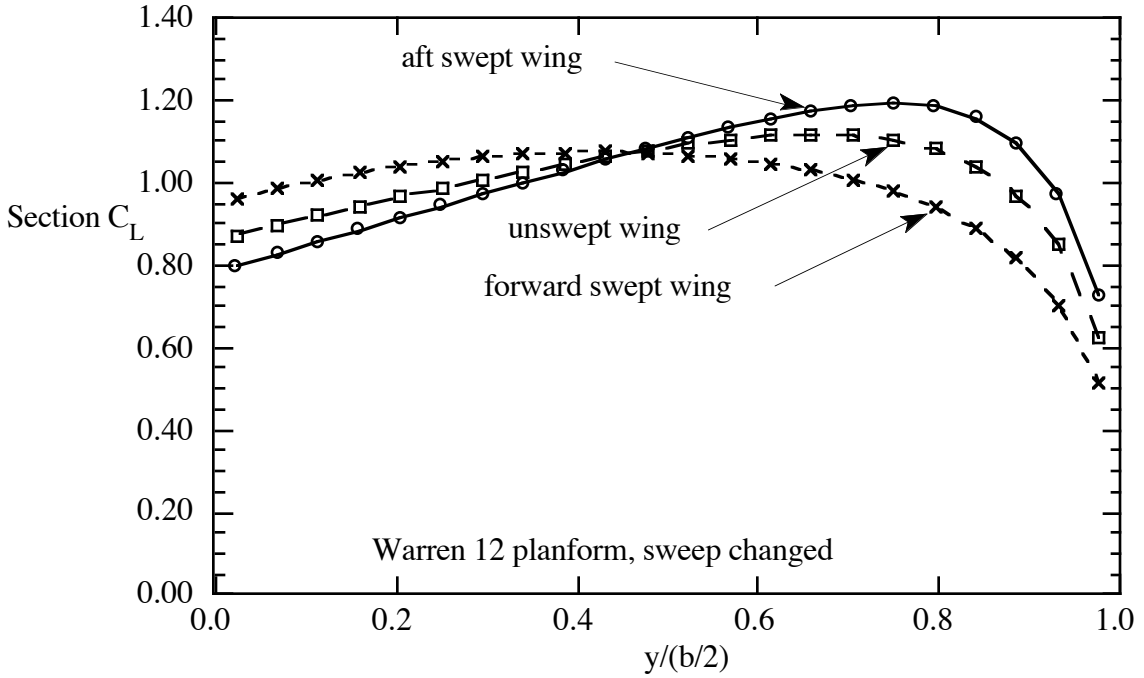

b) comparison of section lift coefficients

Figure 6-36. Effects of sweep on planform spanload and lift coefficient distributions, AR = 2.8.

Similar results are now presented for a series of wings with larger aspect ratios (AR = 8) than the wings used in the study given above. Figure 6-37 shows the planforms used for comparison and Figure 6-38 presents the results for the spanwise distribution of lift and section lift coefficient. These results are similar to the previous results. However, the trends observed above are in fact exaggerated at the higher aspect ratio.

Aerodynamic problems as well as structural penalties arise when using a swept wing. Because of the high section lift coefficient near the tip, aft swept wings tend to stall near the tip first. Since the lift at the tip is generated well aft, the pitching moment characteristics change when the stall occurs. With the inboard wing continuing to lift, a large positive increase in pitching moment occurs when the wingtip stalls. This is known as pitchup, and can be difficult to control, resulting in unsafe flight conditions. Frequently the swept wing pitching moment characteristics are compounded by the effects of flow separation on the outboard control surface. Figure 6-39 provides an example of the pitching moment characteristics of an isolated aspect ratio 10 wing using experimental data.[36] The figure also includes the predictions from **VLMpc**. The agreement is reasonably good at low angle of attack, but deteriorates at high angle of attack as viscous effects become important. This is another reason that sweep is minimized.

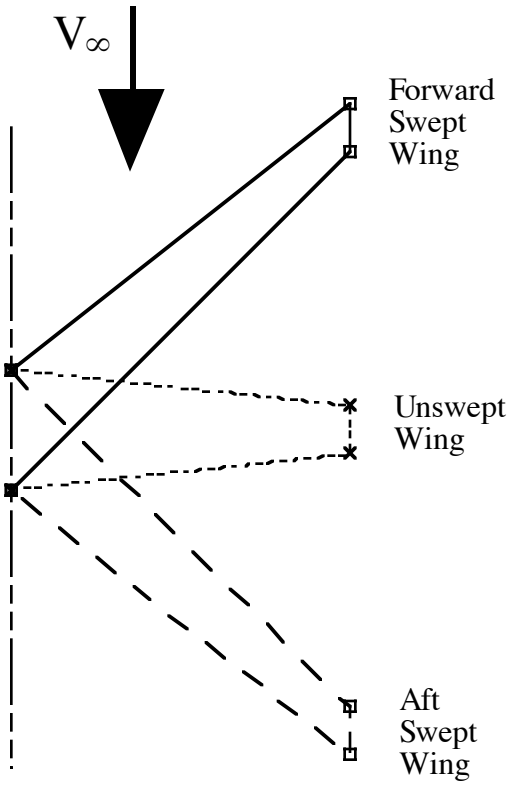

Figure 6-37. Comparison of forward, unswept, and aft swept wing planforms, AR = 8.

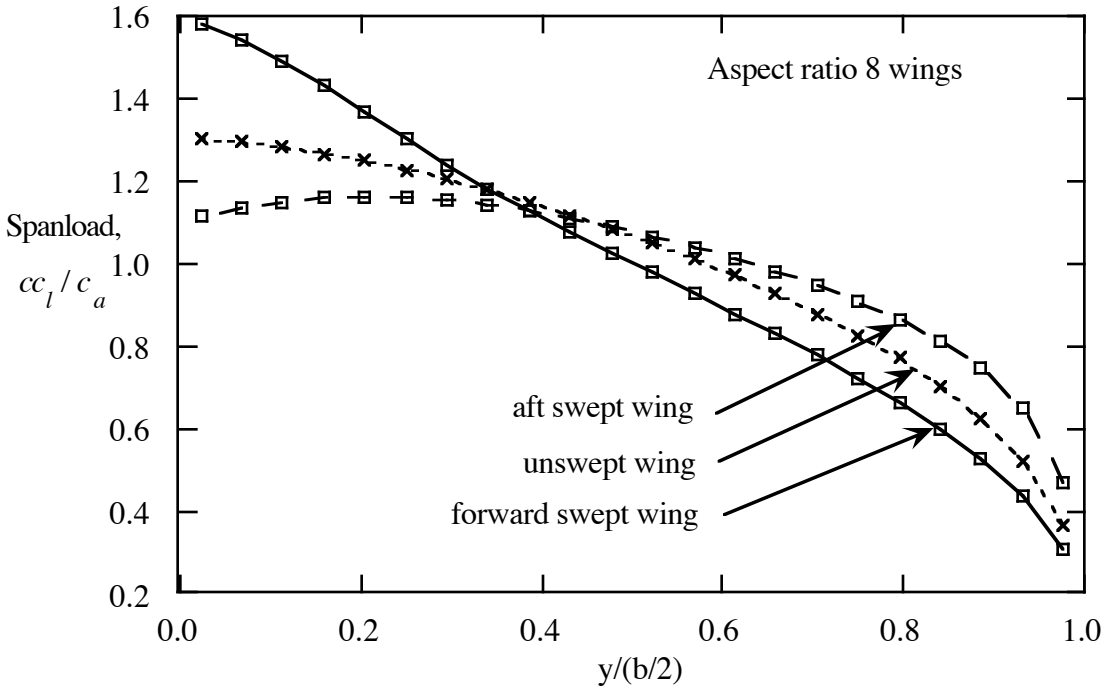

a) comparison of spanloads

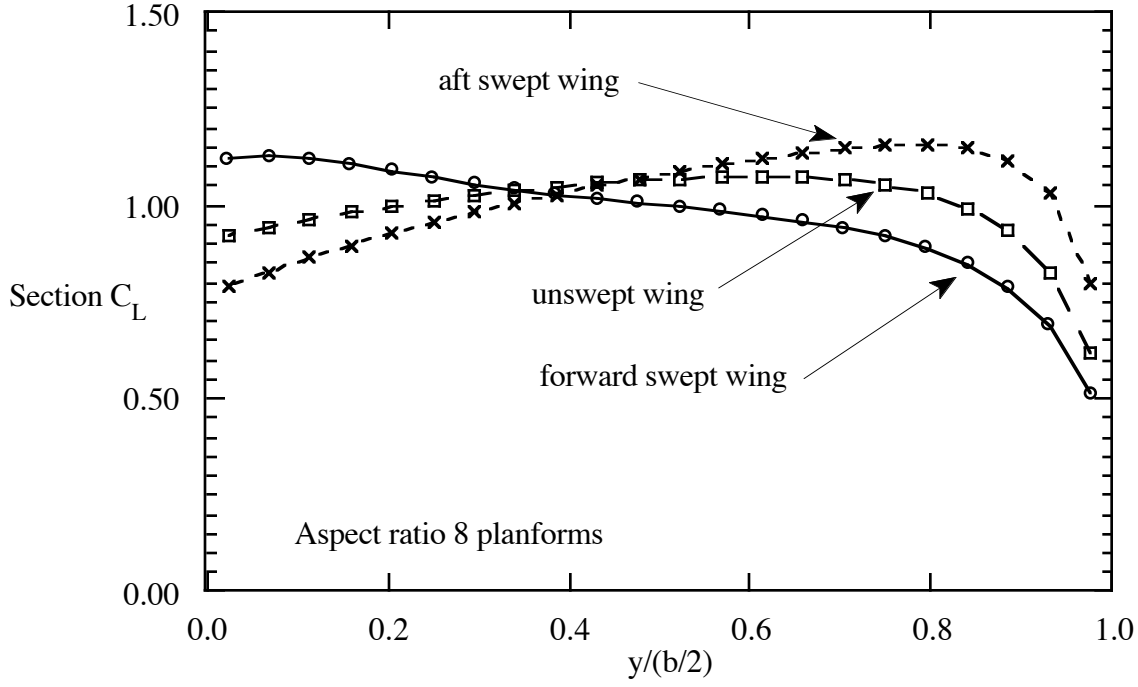

b) comparison of section lift coefficients

Figure 6-38. Effects of sweep on planform spanload and lift coefficient distributions, AR = 8.

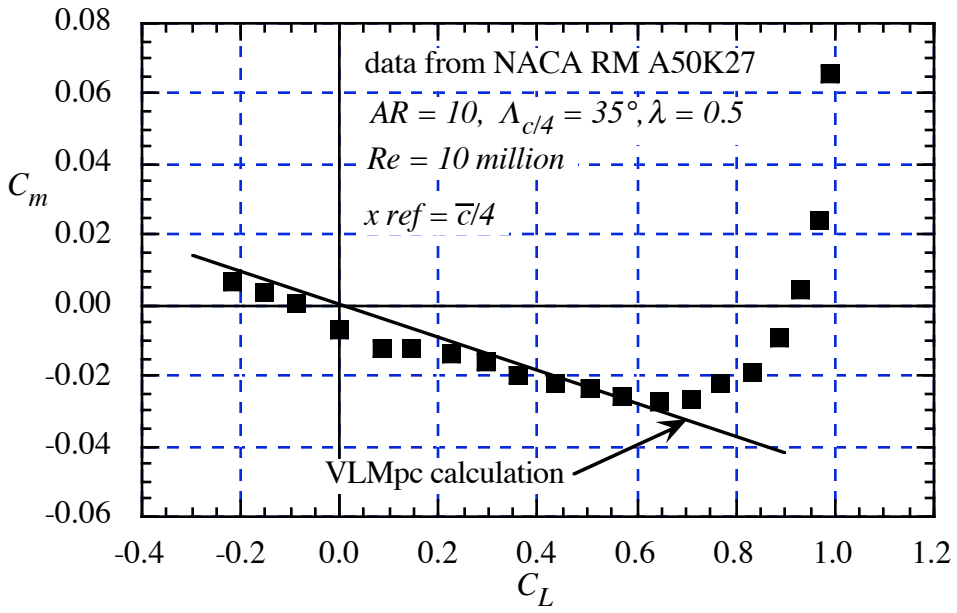

Figure 6-39. Example of isolated wing pitchup: NACA data[36] compared with **VLMpc**.

To control the spanload, the wing can be twisted. Figure 6-40 shows typical twist distributions for aft and forward swept wings, obtained from John Lamar's program **LamDes**.[37] (see the Drag chapter for a description of this code). In each case the twist is used to reduce the highly loaded areas, and increase the loading on the lightly loaded portions of the wing, bringing the spanload to an elliptical shape. For an aft swept wing this means the incidence is increased at the wing root, known as washin, and reduced, known as washout, at the wing tip. Just the reverse is true for the forward swept wing. The sudden drop in required twist at the tip for the forward swept wing case is frequently seen in typical design methods and attributed to a weakness in the method and "faired out" when the aerodynamicist gives his design to the lofting group.

Although geometric sweep is used to reduce the effective Mach number of the airfoil, the geometric sweep is not completely effective. The flowfield resists the sweep. In particular, the wing root and tip regions tend to effectively unsweep the wing. Aerodynamicists study lines of constant pressure on the wing planform known as isobars to investigate this phenomenon. Figure 6-41 presents the computed isobars for a typical swept wing,[38] using a transonic small disturbance method.[39] The effect is dramatic. The effective sweep may actually correspond to the isobar line from the wing root trailing edge to the leading edge at the wing tip. To increase the isobar sweep, in addition to geometric sweep and twist, the camber surface and thickness are typically adjusted to move the isobars forward at the wing root and aft at the wing tip. This is a key part of the aerodynamic wing design job, regardless of the computational, methodology used to obtain the predicted isobar pattern.

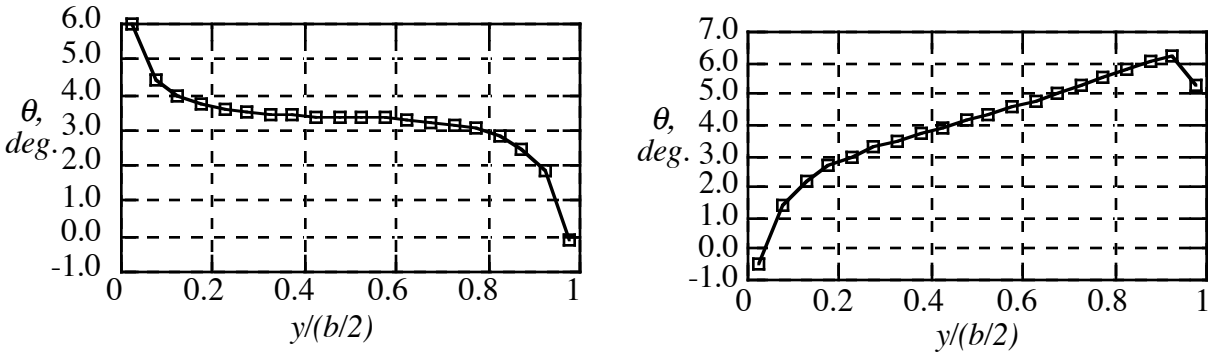

a) aft swept wing b) forward swept wing

Figure 6-40. Typical twist distribution required to improve spanload on swept wings

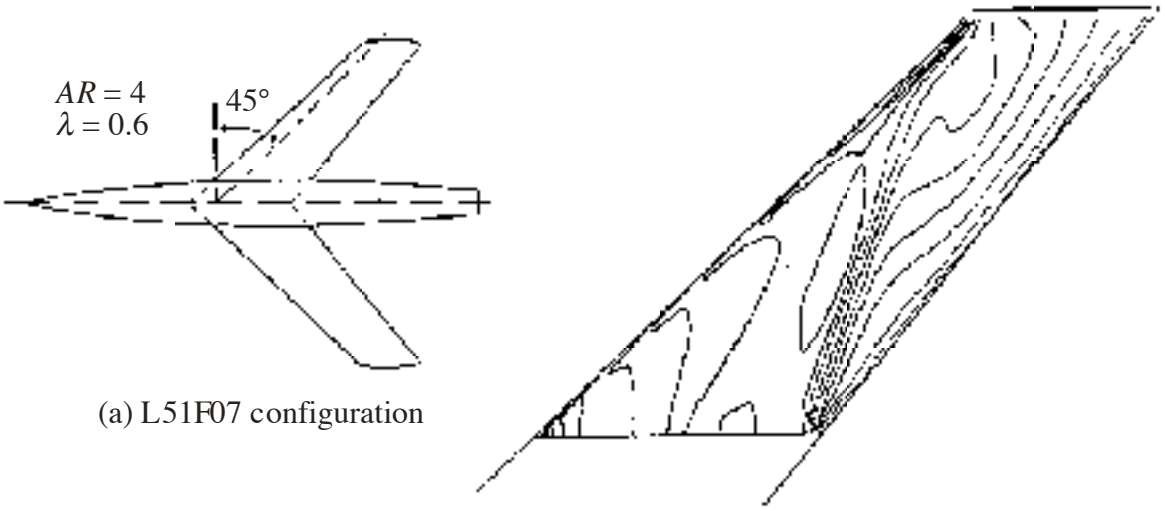

(a) L51F07 configuration

(b) Upper Surface Isobars

Figure 6-41. Example of the isobar distribution on an untwisted swept wing.[39]

Using the wing planform and twist, together with a constant chord loading, Figure 6-42 provides the camber lines required to support the load near the root, the mid-span and the wing tip. These results were also computed using **LamDes**.[37] At each station a similar chord load is specified. We can easily see the differences in the camber required. This is an explicit illustration of the modification to an airfoil camberline required to maintain two-dimensional airfoil-type performance when the airfoil is placed in a swept wing. These modifications represent the explicit effects of the three dimensionality of the flowfield.

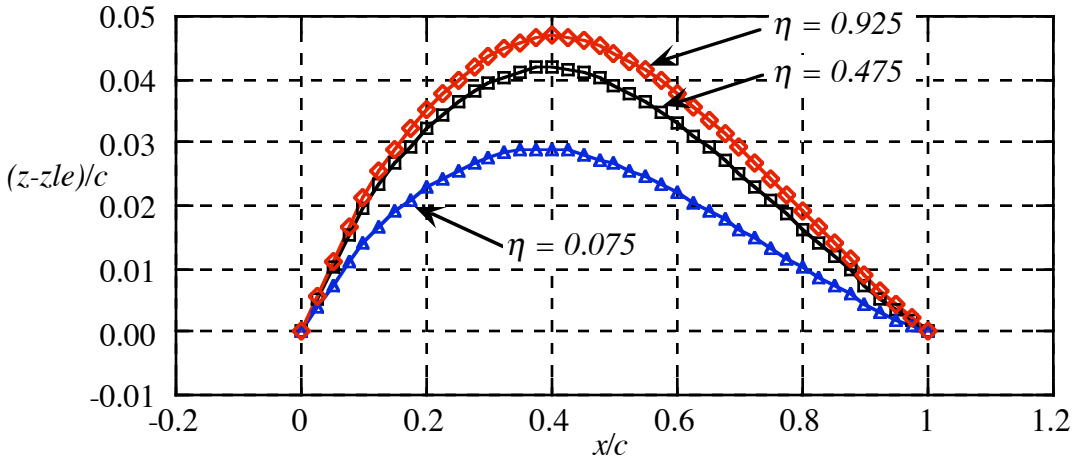

Figure 6-42. Comparison of camber lines required to develop the same chord load shape at the root, mid-span and tip region of an aft swept wing. (from **LamDes**[37])

Many other refinements are available to the aerodynamic designer. Insight into both the human and technical aspects of wing design prior to the introduction of computational aerodynamics is available in two recent books describing the evolution of the Boeing series of jet transports.[40,41] One interesting refinement of swept wings has been the addition of trailing edge area at the wing root. Generally known as a "Yehudi flap", this additional area arises for at least two reasons. The reason cited most frequently is the need to provide structure to attach the landing gear at the proper location. However, the additional chord lowers the section lift coefficient at the root, where wing-fuselage interference can be a problem, and the lower required section lift makes the design job easier. Douglas introduced this planform modification for swept wings on the DC-8, while Boeing did not incorporate it until the -320 model of the 707. However, retired Boeing engineer William Cook, in his book,[40] on page 83, says it was first introduced on the B-29 to solve an interference problem between the inboard nacelle and the fuselage. The aerodynamic benefit to the B-29 can be found in the paper by Snyder.[42] Cook says, in a letter to me, that the device got its name because each wind tunnel part needed a name and there was a popular radio show at the time that featured the continuing punch line "Who's Yehudi?" (the Bob Hope Radio show featuring Jerry Colonna, who had the line). Thus, a Boeing engineer decided to call it a Yehudi flap. This slight extra chord is readily apparent when examining the B-29, but is very difficult to photograph.

6.3.5 The Relation Between Airfoils and Swept Wings

Above we examined the basic aerodynamics of airfoils using panel methods. This section has emphasized the planform shape, and its analysis using vortex lattice methods. The connection between the airfoil and planform is important. In most cases the integration of the airfoil concept and the wing planform concept is crucial to the development of a successful configuration. Simple

sweep theory can be used to provide, at least approximately, the connection between the airfoil and the planform for swept wings. The typical aerodynamic design problem for an airfoil in a wing is defined by specifying the streamwise thickness to chord ratio, t/c, the local section lift coefficient, $C_{l\text{des}}$, and the Mach number. This three-dimensional problem is then converted to a corresponding two-dimensional problem. The desired two dimensional airfoils are then designed and transformed back to the streamwise section to be used as the wing airfoil section. Examples of the validity of this technique, together with details on other properties, including the "cosine cubed" law for profile drag due to lift, are available in the NACA report by Hunton.[43] The relations between the streamwise airfoil properties and the chordwise properties (values normal to the leading edge, as shown in Figure 6-43) are:

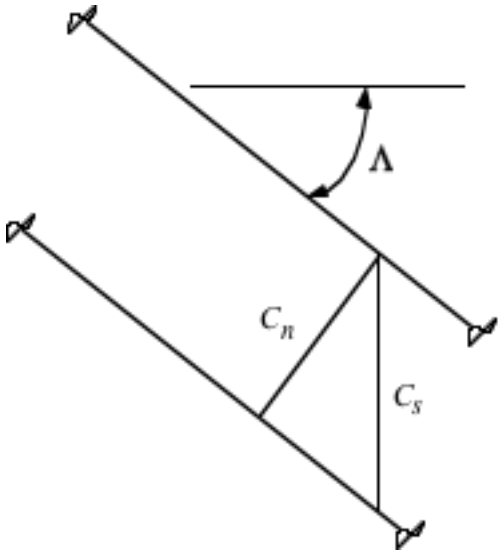

$$C_n = C_s \cos\Lambda$$

$$M_n = M_\infty \cos\Lambda$$

$$t/c)_n = t/c)_s/\cos\Lambda$$

and

$$C_{Ls} = C_{Ln} \cos^2\Lambda$$

Figure 6-43. Definitions connecting the airfoil and wing design problems.

These relations demonstrate that the equivalent two-dimensional airfoil is thicker, operates at a lower Mach number, and at a higher lift coefficient than the related three-dimensional wing airfoil section. Taper effects on real wings require the selection of an effective sweep angle. Numerous approaches have been used to determine the effective angle, where guidance has been obtained by examining experimental data. The quarter chord sweep or shock sweep are typical choices.

One good example of airfoil/planform matching is the Grumman X-29. In that case wind tunnel testing of advanced transonic maneuver airfoil sections on aft swept wing configurations led the aerodynamicists (Glenn Spacht in particular) to conclude that the proper planform to take advantage of the advanced airfoil section performance should be swept forward.

6.3.6 Wing/Tail and Canard/Wing Aerodynamics

Additional lifting surfaces are used to provide control over a wide range of conditions. If modern advanced control systems are not used, the extra surface is also designed, together with the rest of the configuration, to produce a stable design. Considering aft tail configurations first, the problem of pitchup described above for isolated wings must be reconsidered for aft tailled configurations. In particular, T-tail aircraft can encounter problems when the horizontal tail interacts with the wake of the wing at stall. The pitching moment characteristics of the DC-9[44] show an initial abrupt nose-down characteristic is the result of careful design, before a large pitchup develops. Even though pitch-up is a viscous effect, inviscid calculations clearly show why it happens, and can provide valuable information. On the DC-9 a stable trim condition occurs at an angle of attack of 43°. This is an undesirable equilibrium condition, which could result in the vehicle actually trying to "fly" at this angle of attack. If adequate control power is not available, it may even be difficult to dislodge the vehicle from this condition, which is commonly known as a deep or hung stall. This will result in a rapid loss of altitude due to the very high drag. Although for this configuration full down elevator eliminates the possibility of getting "trapped" in a trimmed flight condition at this angle of attack, the amount of pitching moment available may not be sufficient to affect a rapid recovery from this condition. Examples of pitchup characteristics are not readily available. Aerodynamic designers do not like to admit that their configurations might have this characteristic. This aspect of swept wing and wing-tail aerodynamics is an important part of aerodynamic configuration development.

Even low tail placement cannot guarantee that there will not be a problem. The pitching moment characteristics for an F-16 type wind tunnel model[45] showed a deep stall, and in fact the allowable angle of attack on the F-16 is limited by the control system to prevent the airplane from encountering this problem. In this case the pitchup arises because of powerful vortices generated by the strakes, which continue to provide lift as the wing stalls.

Canard configurations provide another interesting example of multiple lifting surface interaction. The downwash from the canard wake, as it streams over the wing, reduces the effective angle of attack on the wing locally, and hence the local lift on the wing behind the canard. Wing twist is used to counteract this effect. Figure 6-44 illustrates how this interaction occurs. The relative loading of the surfaces (how much lift is carried by the canard and how much is carried by the wing) is an important consideration in configuration aerodynamics. The induced drag is highly dependent on the relative wing loading, which is determined by the selection of the configuration stability level and the requirement to trim about the center of gravity. Figure 6-45 shows a wing-canard combination that can be used to illustrate the strong effect of *cg* position on induced drag. Figure 6-46, presents the induced drag computed using **LamDes**,[37] and shows the variation of

trimmed drag changes with *cg* position. Anything above the minimum drag value should be considered the trimmed drag penalty. Three different canard heights are shown for a range of *cg* positions, which is equivalent to varying the stability level. Figure 6-47 provides an example of the wing twist required to account for the effect of the canard downwash. Note that the forward swept wing twist increment due to the canard acts to reduce the twist required, which is exactly opposite the effect for the aft swept wing.

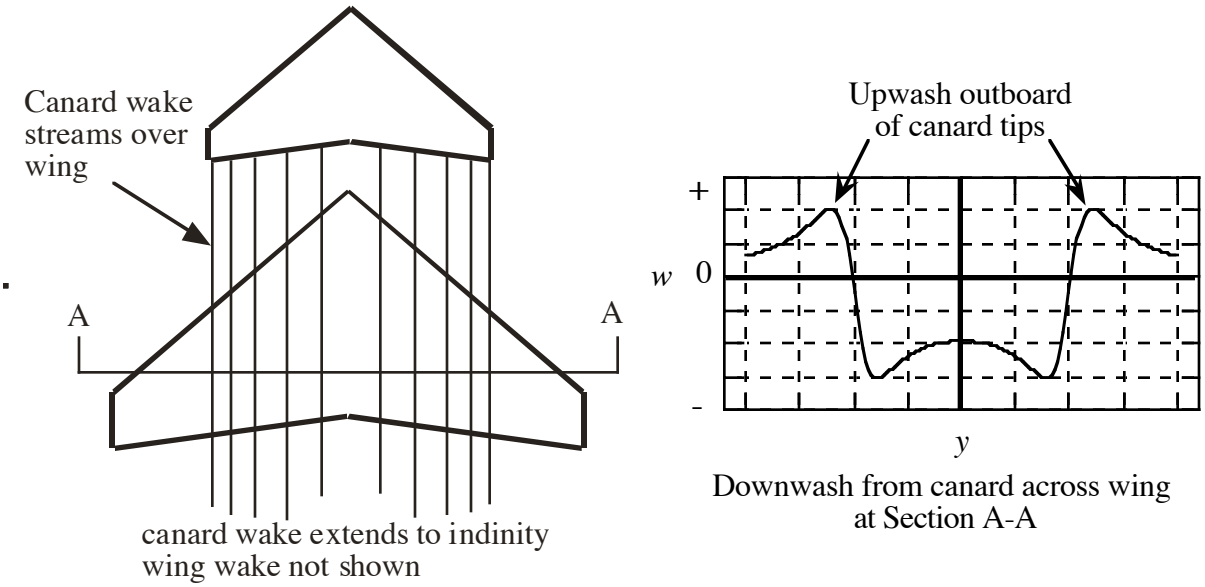

Figure 6-44. Illustration of wing-canard interaction.

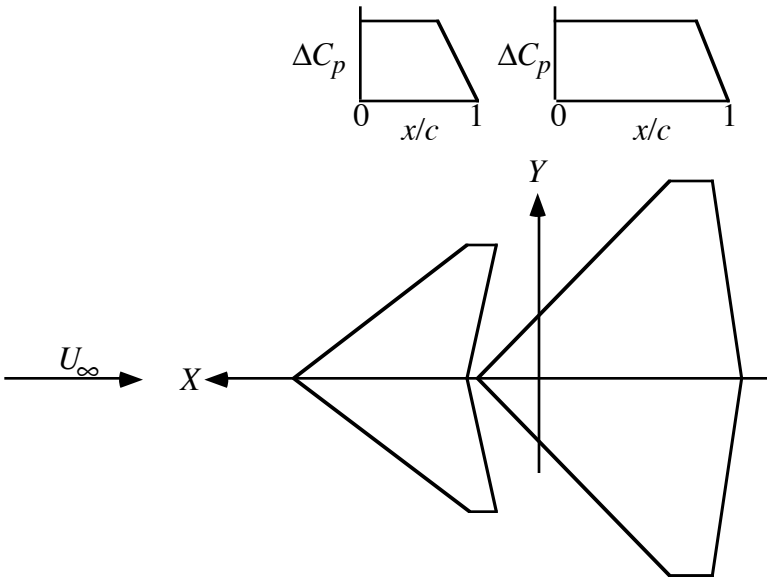

Figure 6-45. Canard-wing planform and chord loads used in example induced drag calculation.

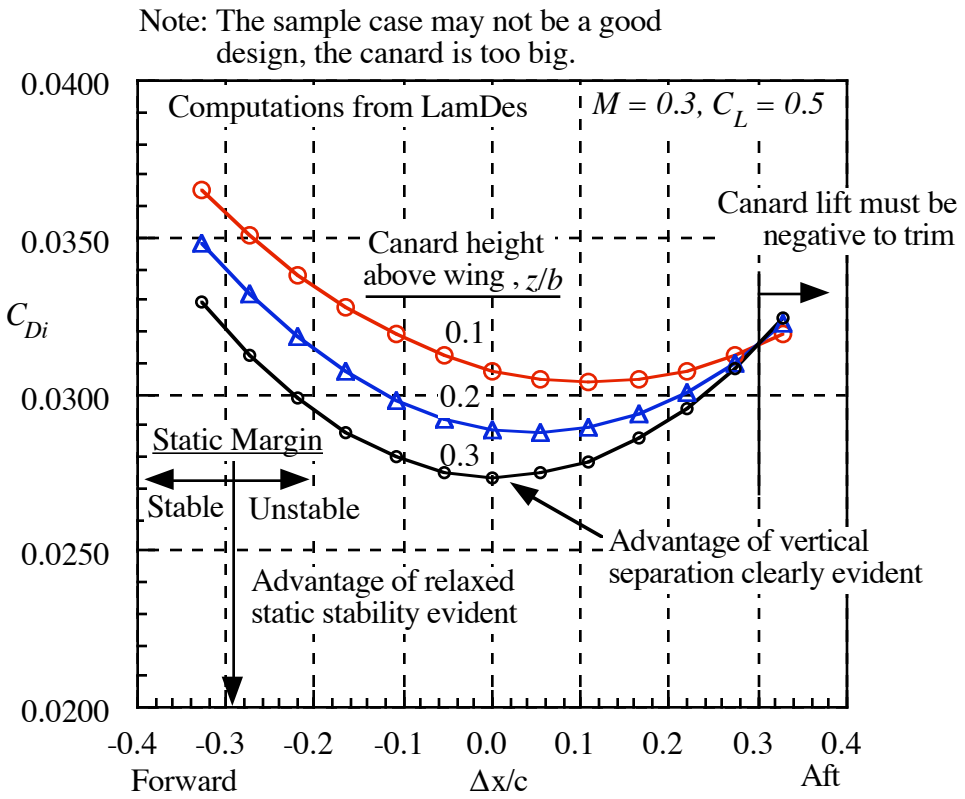

Figure 6-46. Minimum trimmed drag variation with trim position and canard-wing separation, an example of the relation of minimum trimmed drag to balance (stability).[37]

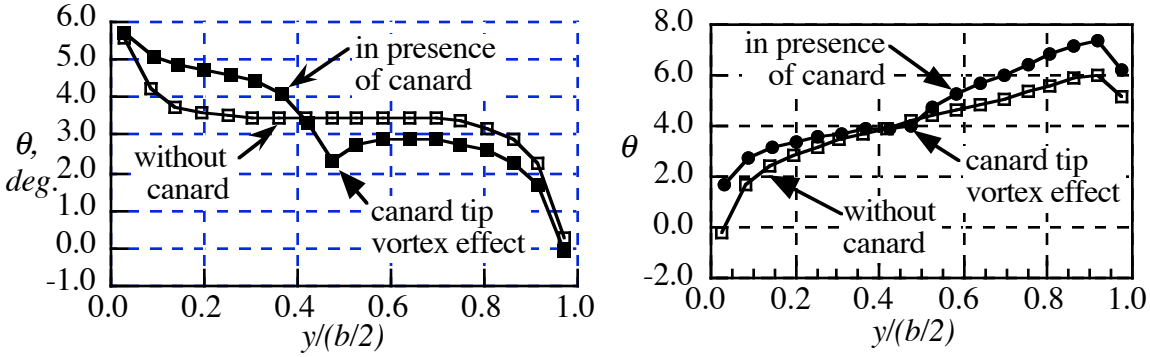

a) aft swept wing b) forward swept wing

Figure 6-47. Effects of canard wake on wing twist requirements. Twist required for minimum drag using LamDes[37] (Note: results depend on configuration details, balance, and the numerics lead to sudden drop in incidence at the wingtip of the forward swept wing, that may or may not be accurate.).

6.3.7 Ground effects using a VLM code

We complete our discussion of wings at subsonic speeds with an example of ground effects, computed using **VLM** methods. Figure 6-48 shows the effects of the presence of the ground on the aerodynamics of simple unswept rectangular wings. The lift and pitching moment slopes are presented for calculations made using **JKayVLM** and compared with the results published by

Kalman, Rodden and Giesing,[46] and experimental data. The agreement between the data and calculations is excellent for the lift curve slope. The $AR = 1$ wing shows the smallest effects of ground proximity because of the three-dimensional relief provided around the wing tips. As the aspect ratio increases, the magnitude of the ground effects increases. The lift curve slope starts to increase rapidly as the ground is approached.

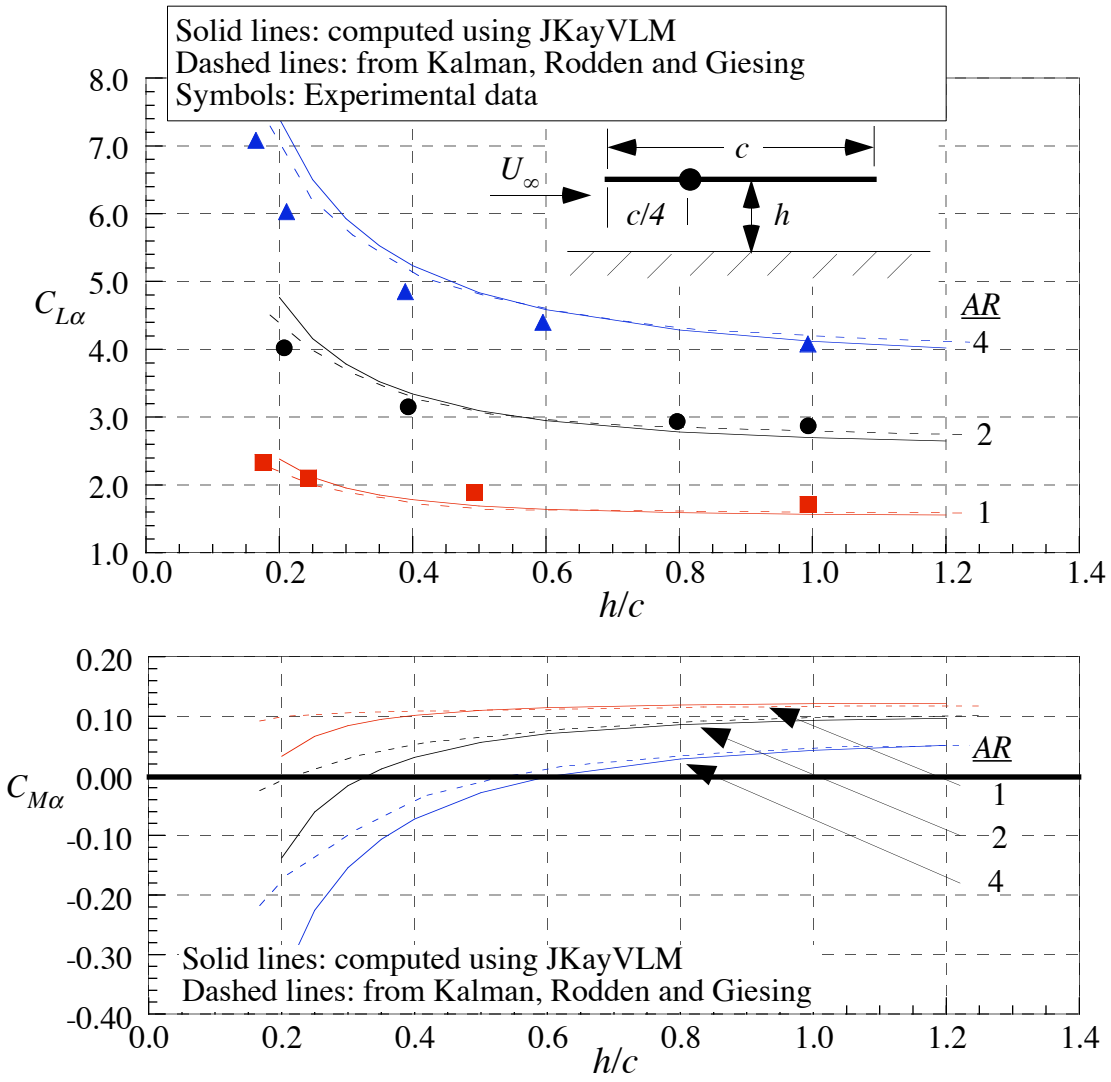

Figure 6-48. Example of ground effects for a simple rectangular wing. **JKayVLM**[15] is compared with a case from Kalman, Rodden and Giesing[46]

The wings also experience a significant change in the pitching moment slope (aerodynamic center shift), and this is also shown. Note that the predictions start to differ as the ground is approached. **JKayVLM** actually rotates the entire surface to obtain another solution to use in estimating the lift curve slope. The standard procedure used by most methods is to simply change the slope condition at the mean line location. Because of the proximity to the ground, this approach might be a case where the application of the boundary condition on the mean line may not be accurate.

Figure 6-49 presents similar information for the effect of dihedral angle on a wing. In this case the effects of anhedral, where the wing tip approach the ground, are extremely large. The results of dihedral changes for a wing out of ground effect are shown for comparison. Both methods agree well with each other, with differences appearing only as the wingtips approach the ground. Here again, **JKayVLM** actually rotates the entire geometry, apparently resulting in an increase in the effects as the tips nearly contact the ground. It also prevents calculations from being obtained as close to the ground as the published results. In making these calculations it was discovered that the wing panel was rotated and not sheared, so that the projected span decreases as the dihedral increases, and this produces much more pronounced changes in the lift curve slope due to the reduction in projected span.

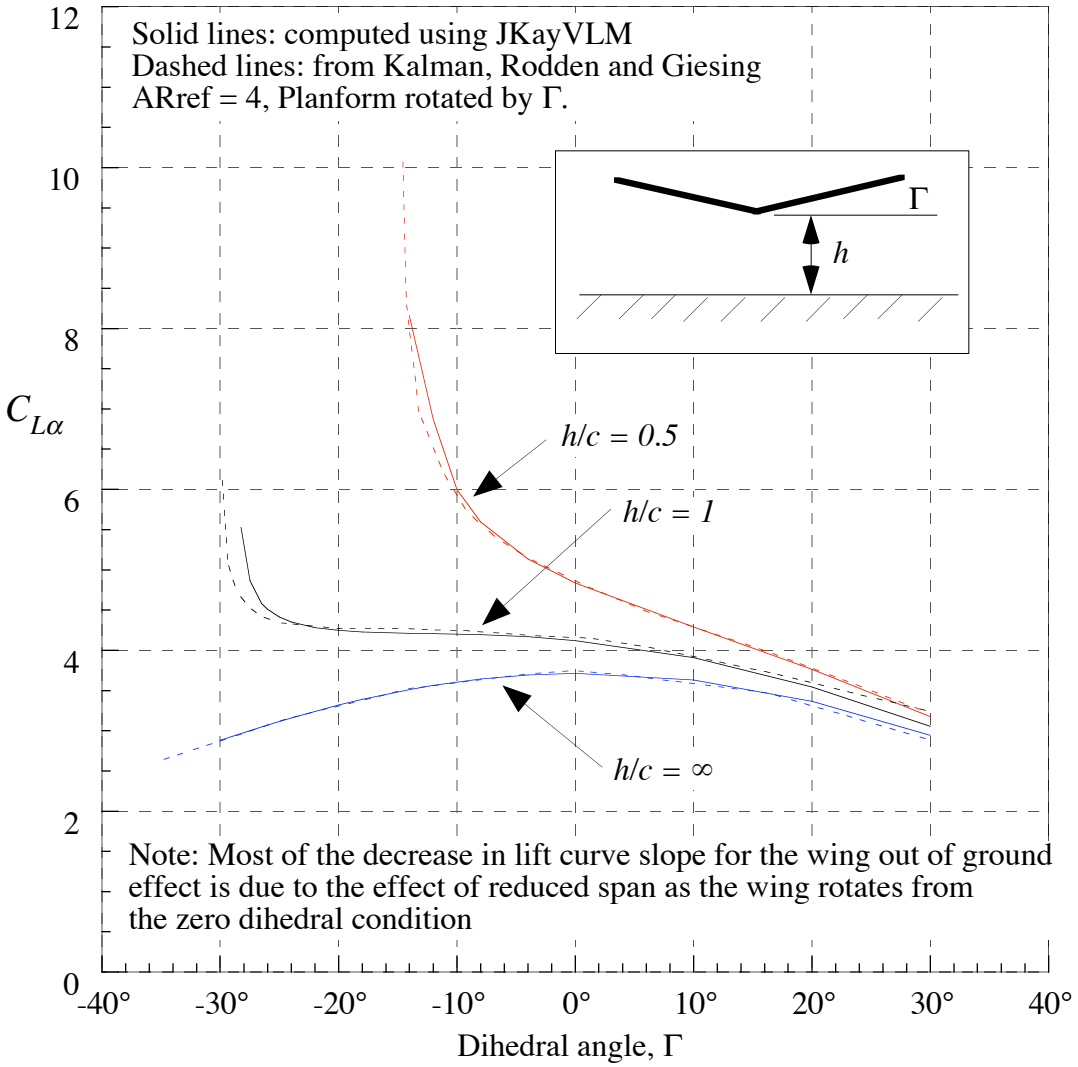

Figure 6-49. Example of ground effects for a wing with dihedral for a case from Kalman, Rodden and Giesing[46] compared with **JKayVLM**[15]

Ground effects shown here arise because of the non-penetration condition at the ground, resulting in generally higher lift slopes. The effect is associated with three-dimensional flow. However, ground effects are considerably more complicated than suggested here. See Torenbeek[47] for a more complete discussion.

6.3.8 Low Aspect Ratio "Slender Wings"

Vortex Flow Effects and the Leading Edge Suction Analogy

For highly swept wings at even moderate angles of attack, the classical attached flow/trailing edge Kutta condition flow model we've adopted is wrong. Instead of the flow remaining attached on the wing and leaving the trailing edge smoothly, the flow separates at the leading edge, forming a well defined vortex. This vortex plays an important role in the design of highly swept, or "slender wing" aircraft. The most notable example of this type of configuration is the Concorde. Sharp leading edges promote this flow phenomena. The basic idea is illustrated in the sketch from Payne and Nelson[48] given here in Figure 6-50.

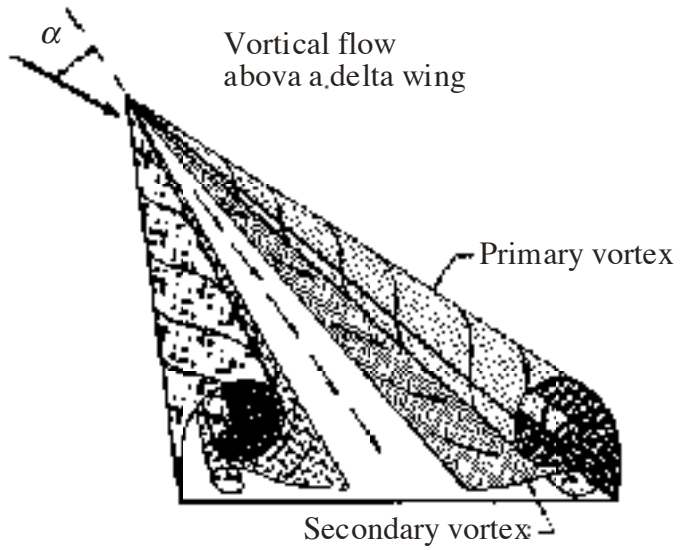

Figure 6-50. Vortex flow development over a delta wing with sharp edges.[48]

An important consequence of this phenomena is the change in the characteristics of the lift generation as the wing angle of attack increases. The vortex that forms above the wing provides an additional low pressure force due to the strongly spiraling vortex flow. The low pressure associated with the centrifugal force due to the vortex leads to the lower pressure on the wing. As the wing increases its angle of attack the vortex gets stronger, further reducing the pressure on the wing. The resulting increase in lift due to the vortex can be large, as shown in Figure 6-51, from Polhamus.[49]

This is an important flow feature. Slender wings have very low attached flow lift curve slopes, and without the additional vortex lift it would be impractical to build configurations with low aspect ratio wings. The low attached flow alone lift curve slope would prevent them from being able to land at acceptable speeds or angle of attack. Vortex lift made the Concorde possible. Another feature of the flow is the high angle of attack at which maximum lift occurs, and typically a very mild lift loss

past maximum lift. These features are a direct result of the leading edge vortex flow structure that occurs on slender wings.

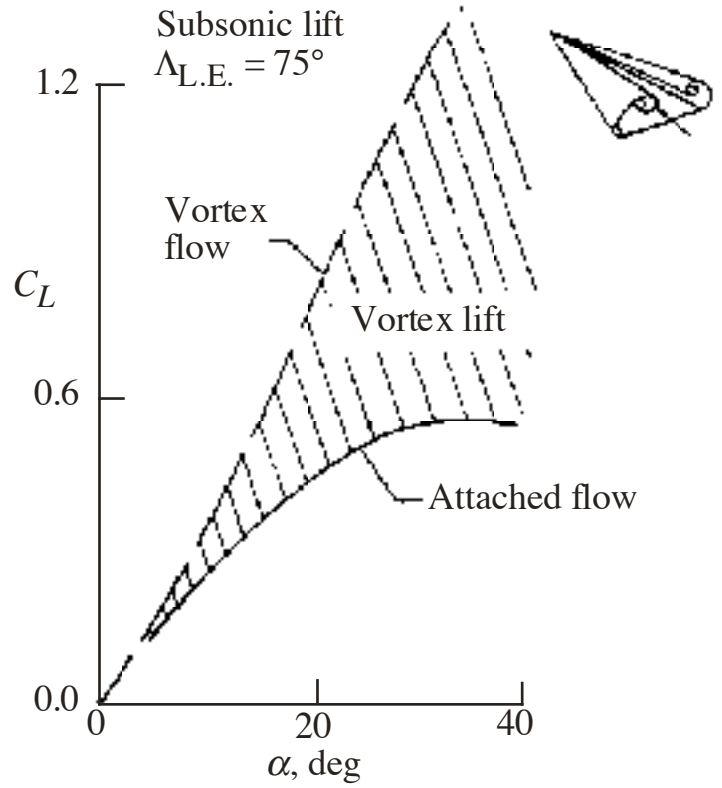

Figure 6-51. Vortex lift changes the characteristic lift development on wings.[49]

Although the vortex lattice method formulation presented above does not include this effect, vortex lattice methods are often used as the basis for extensions that *do* include the leading edge vortex effects. A remarkable, reasonably accurate, flow model for leading edge vortex flows was introduced by Polhamus[50,51] at NASA Langley in 1966 after examining lots of data. This flow model is known as the "Leading Edge Suction Analogy." The concept is quite simple and was invented for sharp edged wings. The leading edge suction that should exist according to attached flow theory is assumed to rotate 90° and generate a vortex induced force instead of a suction when leading edge vortex flow exists. Thus the vortex flow force is assumed to be equal to the leading edge suction force. However, the force now acts in the direction normal to the wing surface in the direction of lift rather than in the plane of the wing leading edge. The concept is shown in the Figure 6-52 from the original Polhamus NASA report.[50] Further details on the effects of vortex flow effects are also available in the reports by Kulfan.[52,53]

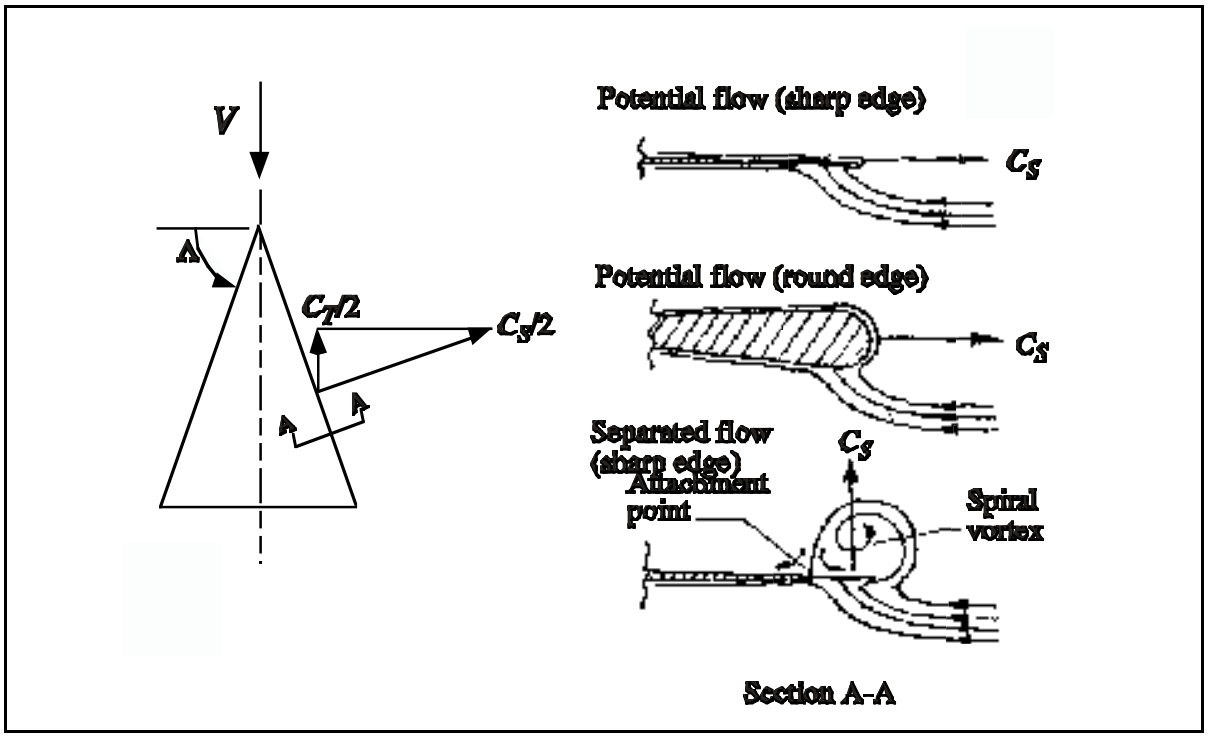

Figure 6-52. The Polhamus leading edge suction analogy.

Polhamus developed charts to compute the suction force for simple wing shapes. For a delta wing with a sharp leading edge, the method is shown compared with the data of Bartlett and Vidal[54] in Figure 6-53. The agreement is quite good (my reconstruction doesn't show agreement as good as that presented by Polhamus,[50] but it is still impressive).

The figure also shows the large size of the vortex lift, and the nonlinear shape of the lift curve when large angles are considered. This characteristic was exploited in the design of the Concorde.

To find the vortex lift using the leading edge suction analogy, an estimate of the leading edge suction distribution is required. However the suction analogy does not result in an actual flowfield analysis including leading edge vortices. The Lamar vortex lattice code (**VLMpc**) optionally includes a fully developed suction analogy based on Polhamus ideas, with extensions to treat side edge suction by John Lamar[7] also included.

Other approaches have been developed to compute leading edge vortex flows in more detail. Many of these methods allow vortex filaments, simulating the leading edge vortices, to leave the leading edge. The location of these vortices, and their effect on the wing aerodynamics as they roll up are explicitly computed. Mook[14] and co-workers are leaders in this methodology.

The area of vortex flows in configuration aerodynamics is fascinating, and an entire conference was held at NASA Langley[55] devoted to the topic. The references cited above were selected to provide an entry to the literature of these flows. Interest in the area remains strong. The effects of round leading edges have been investigated by Ericsson and Reding[56] and Kulfan.[52] The relation between sweep, vortex lift, and vortex strength has been given recently by Hemsch and Luckring. [57]

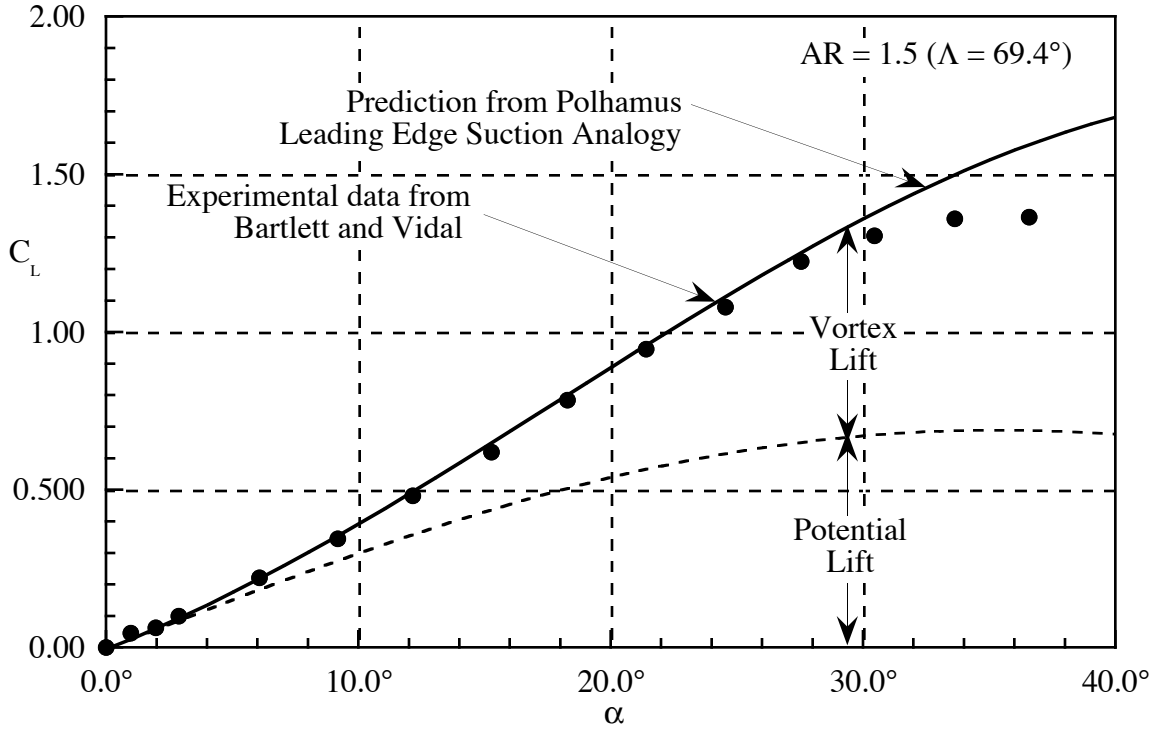

Figure 6-53. Comparison of the leading edge suction analogy with data from Bartlett and Vidal (Ref. 54).

6.4 Exercises

1. Program **PANEL**.

   a) Obtain a copy of program **PANEL** and the sample case.

   b) Convert **PANEL** to run on your PC.

   c) Run the sample case: NACA 4412, 20 pts. upper, 20 pts. lower, α = 4° , and verify against sample case.

   d) Document

      i) compile time required on your PC (cite computer and compiler used)
      ii) the execution time for the sample case
      iii) the accuracy relative to the sample case.
      iv) the exact modifications required to make the code work on your computer

2. Start work on program **PANEL**

   a) Save a reference copy of the working code!

   b) Check convergence with panels (NLOWER+NUPPER must be less than 100 currently). How many panels do you need to get results independent of the number of panels? What happens to the computer time as the number of panels increases?

c) Check the coordinates generated by the airfoil routine vs. exact (consider using the NACA 0012, see App. A for geometry definition), including examination of the coordinates at the trailing edge. This is best done by making a table of exact and computed values at selected values of *x/c*. What did you find out?

d) Locate the source strengths, and sum the source strengths x panel lengths to get the total source strength. Does it sum to zero? Should it?

e) Where is the moment reference center in this code?

Submit an assessment of your findings.

3. Modify program **PANEL**:

You need a version of **PANEL** that will allow you to compute the pressure distribution on arbitrary airfoils. This exercise will give you this capability. Modify the code to interpolate input airfoil points to the program defined surface points, *x/c*. The resulting code should:

a) accept arbitrary airfoil input data

b) echo all the input data on the output

c) generate an output file for post processing

(both for plotting and as the input to a boundary layer code)

d) output *Cm* about the airfoil quarter chord point.

Hint: Don't alter the panel distribution. The paneling scheme should be independent of the input distribution of airfoil coordinates. This produces a much more general and accurate program. This problem is usually solved by finding both the *x/c* and *y/c* values as functions of the airfoil arc length, starting at the lower surface trailing edge. A spline fit is usually used to interpolate the values along the arc length.

Check your modified code. Run the airfoil you ran previously with internal coordinate generation. This time use an input file with the same coordinates as external inputs. Submit a description of your work, and assess your results.

4. Assess the accuracy of incompressible potential flow theory. Run your modified **PANEL** code using the airfoil you selected in the exercise in Chap. 1. (What happens if your airfoil has a trailing edge with finite thickness? What do you do now?)

- compare the computed pressure distribution with the experimental data
- compare the computed force and moment results with the data
(over a range of angles of attack

Turn in a CONCISE report describing the results of your work. Include a plot showing the pressure distribution comparison, and a plot(s) showing comparison with forces and moments. What do you conclude about the accuracy of this method?

5. Airfoil design using program **PANEL**

Take your reference airfoil:

a) add thickness on the bottom (mid chord)- what happens?
b) shave some thickness off the bottom (mid chord) - ?
c) add thickness on the top (mid chord)- what happens?
d) deflect the trailing edge down a couple of degrees
(how sensitive is the airfoil to changes at the TE?)

Hint: use smooth δs to the reference foil employing analytic formulas.

Turn in a CONCISE report comparing the effects on the pressure distribution due to the above modifications.

6. How good is thin airfoil theory? Compare the thin airfoil ΔCp for a flat plate with program **PANEL**.

   Recall thin airfoil theory for an uncambered flat plate:

$$\Delta C_p = 4\alpha\sqrt{\frac{(1-x/c)}{x/c}}\,.$$

   a) pick an NACA 0012 airfoil at $\alpha = 2°$ and 12° and run **PANEL**.
   b) plot $\Delta Cp/\alpha$ as a function of x/c.
   c) how many panels do you need to get a converged solution from **PANEL**?
   d) what conclusions do you reach?

7. Get a copy of **VLMpc** from the web site. The detailed instructions for this program are included on the software, web site. Install the program on your personal computer and repeat the sample case, checking that your output is the same as the sample output files on the web. Study the output to familiarize yourself with the variety of information generated. Turn in a report describing your efforts (not the output), including any mods required to make the code run on your computer.

8. How good is thin airfoil theory? Compare the thin airfoil theory ΔCp for a 2D flat plate airfoil with program **VLMpc**.

   Flat plate thin airfoil theory:

$$\Delta C_P = 4\alpha\sqrt{\frac{(1-x/c)}{x/c}}$$

   i. Pick an aspect ratio 10 unswept wing at $\alpha = 3°$ and 12° and run **VLMpc**.
   ii. Plot $(\Delta Cp)/\alpha$ as a function of x/c at the wing root.
   iii. How many panels do you need to get a converged solution from **VLM**?
   iv. What conclusions do you reach?

9. Compare the validity of an aerodynamic strip theory using **VLMpc**. Consider an uncambered, untwisted wing, AR = 4, λ = .4, Λ_{le} = 50°, at a lift coefficient of 1.0. Plot the spanload, and the ΔC_p distribution at approximately the center section, the midspan station, and the 85% semispan station. Compare your results with a spanload constructed assuming that the wing flow is approximated as 2D at the angle of attack required to obtain the specified lift. Also compare the chordloads, ΔC_p, at the three span stations. How many panels do you need to obtain converged results. Document your results. Do you consider this aerodynamic strip theory valid based on this investigation? Comment.

10. Compare the wing aerodynamic center location relative to the quarter chord of the *mac* for the wing in exercise 9, as well as similar wings. Consider one wing with zero sweep on the quarter chord, and a forward swept wing with a leading edge sweep of -50°. Compare the spanloads. Document and analyze these results. What did you learn from this comparison?

11. For the wings in exercise 10, compare the section lift coefficients. Where would each one stall first? Which wing appears to able to reach the highest lift coefficient before the section stalls.
12. For the problem in exercise 11, add twist to each wing to obtain near elliptic spanloads. Compare the twist distributions required in each case.
13. Pick a NASA or NACA report describing wind tunnel results for a simple one or two lifting surface configuration at subsonic speeds. Compare the lift curve slope and stability level predicted by **VLMpc** with wind tunnel data. Submit a report describing your work and assessing the results.
14. Add a canard to the aft and forward swept wings analyzed in exercise 10. Plot the sum of the spanloads. How does the canard effect the wing spanload.
15. Consider the wings in exercise 14. How does lift change with canard deflection? Add an equivalent tail. Compare the effect of tail or canard deflection on total lift and moment. Did you learn anything? What?
16. Construct a design code using the 1/4 - 3/4 rule and compare with **DESCAM**.
17. Construct a little 2D code to study ground effects.
18. Compare wing and wing/tail(canard) results for $C_{L\alpha}$ with standard analytic formulas.

6.5 References

[1] Hess, J. L., "Panel Methods in Computational Fluid Dynamics," *Annual Review of Fluid Mechanics*, Vol. 22, 1990, pp. 255-274.

[2] Hess, J.L., "Linear Potential Schemes," *Applied Computational Aerodynamics*, P.A. Henne, ed., AIAA, Washington, 1990. pp.21-36.

[3] Erickson, L.L., "Panel Methods—An Introduction," NASA TP-2995, Dec. 1990.

[4] Katz, J., and Plotkin, A., *Low-Speed Aerodynamics From Wing Theory to Panel Methods*, 2nd Edition, Cambridge University Press, 2001.

[5] *Vortex Lattice Utilization Workshop*, NASA SP-405, May, 1976

[6] Margason, R.J., and Lamar, J.E., "Vortex-Lattice FORTRAN Program for Estimating Subsonic Aerodynamic Characteristics of Complex Planforms," NASA TN D-6142, 1971

[7] Lamar, J.E., and Gloss, B.B., "Subsonic Aerodynamic Characteristics of Interacting Lifting Surfaces With Separated Flow Around Sharp Edges Predicted by a Vortex-Lattice Method," NASA TN D-7921,1975 http://www.aoe.vt.edu/~mason/Mason_f/MRsoft.html#VLMpc

[8] Lamar, J.E., and Herbert, H.E., "Production Version of the Extended NASA-Langley Vortex Lattice FORTRAN Computer Program," Vol. I, User's Guide, (requires update packet, July, 1984) NASA TM 83303, 1982

[9] Herbert, H.E, and Lamar, J.E., "Production Version of the Extended NASA-Langley Vortex Lattice FORTRAN Computer Program," Vol. II, Source Code, NASA TM 83304, 1982

[10] Lan, C.E., "A Quasi-Vortex-Lattice Method in Thin Wing Theory", *Journal of Aircraft*, Vol. 11, No. 9, September 1974, pp. 518-527.

[11] Hough, Gary R., "Remarks on Vortex-Lattice Methods," *Journal of Aircraft*, Vol. 10, No. 5, May 1973, pp. 314-317.

[12] DeJarnette, F.R., "Arrangement of Vortex Lattices on Subsonic Wings," in *Vortex Lattice Utilization Workshop*, NASA SP-405, May, 1976. pp. 301-319.

[13] Frink, Neal T., "Lifting-Surface Theory for Skewed and Swept Subsonic Wings," *Journal of Aircraft*, Vol. 19, No. 7, July 1982, pp. 519-524.

[14] Mook, D.T., and Nayfeh, A.H., "Application of the Vortex-Lattice Method to High-Angle-of-Attack Subsonic Aerodynamics," SAE Paper No. 851817, October, 1985.

[15] Jacob Kay, W.H. Mason, W. Durham, F. Lutze and A. Benoliel, "Control Power Issues in Conceptual Design: Critical Conditions, Estimation Methodology, Spreadsheet Assessment, Trim and Bibliography," VPI-Aero-200, November 1993. http://www.aoe.vt.edu/~mason/Mason_f/MRsoft.html#ControlPower

[16] Tomas Melin, "Tornado", KTH, Stockholm, Sweden, Master's Thesis and continued development. http://www.flyg.kth.se/divisions/aero/software/tornado/

[17] Mark Drela and Harold Youngren, AVL, http://web.mit.edu/drela/Public/web/avl/

[18] Moran, J. *An Introduction to Theoretical and Computational Aerodynamics*, John Wiley & Sons, New York, 1984. pp. 103-112, 118-123, 260-287. (now reprinted by Dover)

[19] Drela, M. "XFOIL: An Analysis and Design System for Low Reynolds Number Airfoils," in *Low Reynolds Number Aerodynamics*, T.J. Muelle, ed., Lecture Notes in Engineering #54, Springer-Verlag, 1989. http://raphael.mit.edu/xfoil

[20] Abbott, I.H., and von Doenhoff, A.E., *Theory of Wing Sections*, Dover, New York, 1959.

[21] Jones, R.T., *Wing Theory*, Princeton University Press, Princeton, 1990.

[22] Warner, E.P., *Airplane Design: Performance*, McGraw-Hill, New York, 1936.

[23] McGhee, Robert J., and Beasley, William D., "Low Speed Aerodynamic Characteristics of a 17-Percent-Thick Airfoil Section Designed for General Aviation Applications," NASA TN D-7428, 1973.

[24] Ronald D. Joslin, "Aircraft Laminar Flow Control," *Annual Review of Fluid Mechanics*, Vol. 30, pp. 1-29. 1998.

[25] A.L. Braslow, D.V. Maddalon, D.W. Bartlett and R.D. Wagner, "Applied Aspects of Laminar-Flow Technology," *Viscous Drag Reduction in Boundary Layers*, Dennis M. Bushnell, and Jerry N. Hefner, editors, Progress in Astronautics and Aeronautics, Vol. 123, AIAA, Washington, 1990, pp. 47-78.

[26] Kroo, Ilan, "Aerodynamic Analyses for Design and Education," AIAA Paper 92-2664, June 1992. http://www.desktopaero.com/

[27] Volpe, G., "Inverse Airfoil Design: A Classical Approach Updated for Transonic Applications," in *Applied Computational Aerodynamics*, ed. by P.A. Henne, AIAA Progress in Astronautics and Aeronautics, Vol. 125, AIAA, New York, 1990, pp. 191-220.

[28] Labrujere, Th. E., and Sloof, J.W., "Computational Methods for the Aerodynamic Design of Aircraft Components, *Ann. Rev. of Fluid Mech.*, 1993, Vol. 25, pp.183-214.

[29] Bristow, D.R., "A New Surface Singularity Method for Multi-Element Airfoil Analysis and Design," AIAA Paper 76-20, Jan. 1976.

[30] Aidala, P.V., Davis, W.H., Jr., and Mason, W.H., "Smart Aerodynamic Optimization," AIAA Paper 83-1863, July 1983.

[31] Robert H. Liebeck,, "Subsonic Airfoil Design," in *Applied Computational Aerodynamics*, ed. by P.A. Henne, AIAA Progress in Astronautics and Aeronautics, Vol. 125, AIAA, New York, 1990, pp. 133-165.

[32] Mark Drela, "Elements of Airfoil Design Methodology," in *Applied Computational Aerodynamics*, ed. by P.A. Henne, AIAA Progress in Astronautics and Aeronautics, Vol. 125, AIAA, New York, 1990, pp. 191-220.

[33] Gil Crouse, "Airfoil Optimizer," DaVinci Technologies, www.davincitechnologies.com.

[34] Thomas, R.W., "Analysis of Aircraft Stability and Control Design Methods," AFWAL-TR-84-3038, Vol. II, App. B., "Evaluation of Aerodynamic Panel Methods," by John Koegler, May, 1984.

[35] Küchemann, D., *The Aerodynamic Design of Aircraft*, Pergamon Press, Oxford, 1978.

[36] Tinling, B.E., and Kolk, W. R., "The Effects of Mach Number and Reynolds Number on the Aerodynamic Characteristics of Several 12-Percent-Thick Wings Having 35° of Sweepback and Various Amounts of Camber," NACA RM A50K27, Feb. 1951.

[37] Lamar, J.E., "A Vortex Lattice Method for the Mean Camber Shapes of Trimmed Non-Coplanar Planforms with Minimum Vortex Drag," NASA TN D-8090, June 1976.

[38] Loving, D.L., and Estabrooks, B.B., "Transonic Wing Investigation in the Langley Eight Foot High Speed Tunnel at High Subsonic Mach Numbers and at Mach Number of 1.2," NACA RM L51F07, 1951.

[39] Mason, W.H., MacKenzie, D.A., Stern, M.A., Ballhaus, W.F, Jr., and Frick, J., "Automated Procedure for Computing the Three-Dimensional Transonic Flow Over Wing-Body Combinations, including Viscous Effects," Vol. I, Description of Methods and Applications, AFFDL-TR-77-122, February 1978.

[40] Cook, William C., *The Road to the 707*, TYC Publishing, Bellevue, 1991.

[41] Irving, Clive, *Wide-Body: The Triumph of the 747*, William Morrow, New York, 1993.

[42] Snyder, George, "Structural Design Problems in the B-29 Airplane," *Aeronautical Engineering Review*, Feb. 1946, pp. 9-12.

[43] Hunton, Lynn W., "A Study of the Application of Airfoil Section Data to the Estimation of the High-Subsonic-Speed Characteristics of Swept Wings," NACA RM A55C23, June 1955.

[44] Shevell, R.S., and Schaufele, R.D., "Aerodynamic Design Features of the DC-9," *Journal of Aircraft*, Vol. 3, No. 6, Nov.-Dec. 1966, pp. 515-523.

[45] Nguyen, L.T., Ogburn, M.E., Gilbert, W.P., Kibler, K.S., Brown, P.W., and Deal, P.L., "Simulator Study of Stall/Post-Stall Characteristics of a Fighter Airplane With Relaxed Longitudinal Static Stability," NASA TP 1538, Dec. 1979.

[46] Kalman, T.P., Rodden, W.P., and Giesing, J., "Application of the Doublet-Lattice Method to Nonplanar Configurations in Subsonic Flow," *Journal of Aircraft*, Vol. 8, No. 6, June 1971, pp. 406-415.

[47] Egbert Torenbeek, *Synthesis of Subsonic Airplane Design*, Delft University Press, 1981, pp. 551-554.

[48] Payne, F.W., and Nelson, R.C., "An Experimental Investigation of Vortex Breakdown on a Delta Wing," in *Vortex Flow Aerodynamics*, NASA CP 2416, 1985.

[49] Polhamus, E.C., "Application of Slender Wing Benefits to Military Aircraft," AIAA Wright Brothers Lecture, AIAA-83-2566, 1983..

[50] Polhamus, E.C., "A Concept of the Vortex Lift on Sharp Edge Delta Wings Based on a Leading-edge Suction Analogy," NASA-TN 3767, 1966.

[51] Polhamus, E.C., "Prediction of Vortex Lift Characteristics by a Leading-edge Suction Analogy,", *Journal of Aircraft*, Vol. 8, No. 4, 1971, pp. 193-199.

[52] Kulfan, R.M., "Wing Airfoil Shape Effects on the Development of Leading-Edge Vortices," AIAA 79-1675, 1979.

[53] Kulfan, R.M., "Wing Geometry Effects on Leading Edge Vortices," AIAA Paper No. 79-1872, 1979.

[54] Bartlett, G.E., and Vidal, R.J., "Experimental Investigation of Influence of Edge Shape on the Aerodynamic Characteristics of Low Aspect Ratio Wings at Low Speeds," *Journal of the Aeronautical Sciences*, Vol. 22, No. 8, August, 1955, pp.517-533,588.

[55] *Vortex Flow Aerodynamics*, NASA SP-2416 (volume I), and NASA SP-2417 (volume II), October, 1985.

[56] Ericsson, L.E., and Reding, J.P., "Nonlinear Slender Wing Aerodynamics," AIAA Paper No. 76-19, January, 1976.

[57] Hemsch, M.J., and Luckring, J.M., "Connection Between Leading-Edge Sweep, Vortex Lift, and Vortex Strength for Delta Wings," *Journal of Aircraft*, Vol. 27, No. 5, May 1990, pp. 473-475.